HAL
open science

Generation of excitatory and inhibitory neurons from common progenitors via Notch signaling in the cerebellum

Tingting Zhang, Tengyuan Liu, Natalia Mora, Justine Guegan, Mathilde Bertrand, Ximena Contreras, Andi H Hansen, Carmen Streicher, Marica Anderle, Natasha Danda, et al.

To cite this version:

Tingting Zhang, Tengyuan Liu, Natalia Mora, Justine Guegan, Mathilde Bertrand, et al.. Generation of excitatory and inhibitory neurons from common progenitors via Notch signaling in the cerebellum. Cell Reports, 2021, 35 (10), pp.109208. 10.1016/j.celrep.2021.109208 . hal-03256874

HAL Id: hal-03256874

https://hal.sorbonne-universite.fr/hal-03256874

Submitted on 10 Jun 2021

HAL is a multi-disciplinary open access archive for the deposit and dissemination of scientific research documents, whether they are published or not. The documents may come from teaching and research institutions in France or abroad, or from public or private research centers.

L'archive ouverte pluridisciplinaire **HAL**, est destinée au dépôt et à la diffusion de documents scientifiques de niveau recherche, publiés ou non, émanant des établissements d'enseignement et de recherche français ou étrangers, des laboratoires publics ou privés.

Cell Reports

Article

Generation of excitatory and inhibitory neurons from common progenitors via Notch signaling in the cerebellum

Graphical abstract

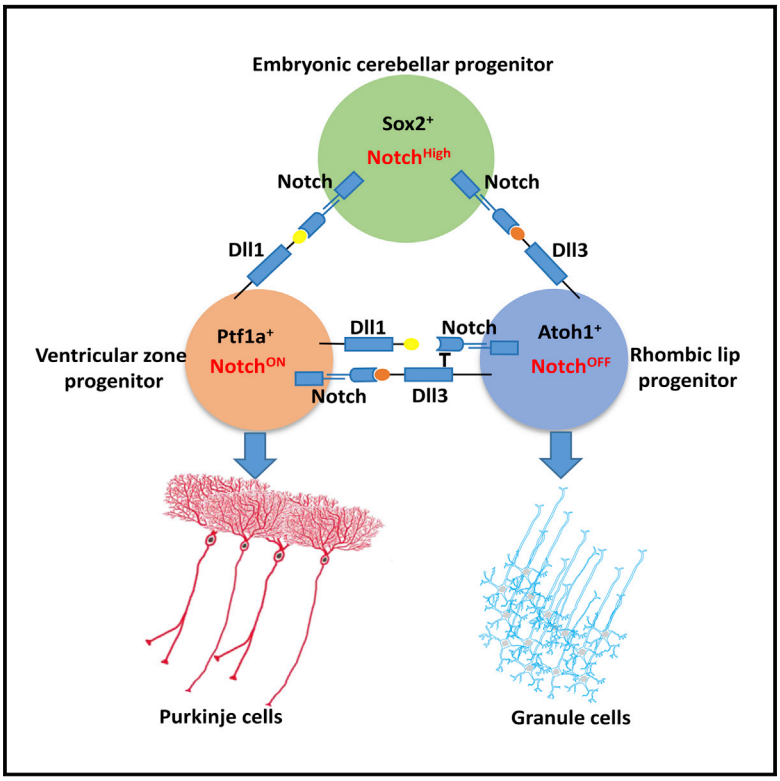

Authors

Tingting Zhang, Tengyuan Liu, Natalia Mora, ..., Luca Tiberi, Simon Hippenmeyer, Bassem A. Hassan

Correspondence

bassem.hassan@icm-institute.org

In brief

Zhang et al. report that excitatory and inhibitory neurons of the cerebellum can arise from individual embryonic cerebellar progenitors (ECPs). Notch activity controls the fate of bi-potential ECP daughters whereby cells with higher Notch activity adopt an inhibitory cell fate, whereas cells with lower Notch activity adopt an excitatory fate.

Highlights

- GABAergic and glutamatergic cerebellar neurons are generated from Sox2$^+$ progenitors
- Single Sox2$^+$ ECPs can give rise to both excitatory and inhibitory cerebellar neurons
- Notch activity mediates GABAergic versus glutamatergic cell fates in Sox2$^+$ ECPs

Zhang et al., 2021, Cell Reports *35*, 109208
June 8, 2021 © 2021 The Authors.
https://doi.org/10.1016/j.celrep.2021.109208

CellPress

Cell Reports

CellPress
OPEN ACCESS

Article

Generation of excitatory and inhibitory neurons from common progenitors via Notch signaling in the cerebellum

Tingting Zhang,[1,2] Tengyuan Liu,[1,2] Natalia Mora,[1,5] Justine Guegan,[1] Mathilde Bertrand,[1] Ximena Contreras,[3] Andi H. Hansen,[3] Carmen Streicher,[3] Marica Anderle,[4] Natasha Danda,[1] Luca Tiberi,[4] Simon Hippenmeyer,[3] and Bassem A. Hassan[1,6,*]

[1]Institut du Cerveau (ICM), Sorbonne Université, INSERM, CNRS, Hôpital Pitié-Salpêtrière, Paris, France
[2]Doctoral School of Biomedical Sciences, KU Leuven, 3000 Leuven, Belgium
[3]Institute of Science and Technology Austria, Am Campus 1, 3400 Klosterneuburg, Austria
[4]Armenise-Harvard Laboratory of Brain Disorders and Cancer, CIBIO, University of Trento, Via Sommarive 9, 38123 Trento, Italy
[5]Present address: Department of Molecular Neurobiology, Donders Institute for Brain, Cognition and Behaviour and Faculty of Science, Radboud University, Nijmegen, the Netherlands
[6]Lead contact
*Correspondence: bassem.hassan@icm-institute.org
https://doi.org/10.1016/j.celrep.2021.109208

SUMMARY

Brain neurons arise from relatively few progenitors generating an enormous diversity of neuronal types. Nonetheless, a cardinal feature of mammalian brain neurogenesis is thought to be that excitatory and inhibitory neurons derive from separate, spatially segregated progenitors. Whether bi-potential progenitors with an intrinsic capacity to generate both lineages exist and how such a fate decision may be regulated are unknown. Using cerebellar development as a model, we discover that individual progenitors can give rise to both inhibitory and excitatory lineages. Gradations of Notch activity determine the fates of the progenitors and their daughters. Daughters with the highest levels of Notch activity retain the progenitor fate, while intermediate levels of Notch activity generate inhibitory neurons, and daughters with very low levels of Notch signaling adopt the excitatory fate. Therefore, Notch-mediated binary cell fate choice is a mechanism for regulating the ratio of excitatory to inhibitory neurons from common progenitors.

INTRODUCTION

Correct brain function depends on neuronal diversity, whereby neurons of different morphologies and physiologies connect to produce functional neuronal circuits. In turn, neuronal diversity is generated from a relatively small and temporally limited number of progenitor cells, or developmental neural stem cells. A major challenge in neurobiology is to understand how progenitors endow their daughters with different cell fates. The study of neurogenesis in a variety of models of vertebrates like zebrafish and mouse, as well as invertebrates like *C. elegans* and *Drosophila*, has converged on three major processes as key to understanding neuronal diversification. First, in both systems, temporal mechanisms ensure that progenitors change competence over time to give rise to different types of neurons during brain development, as has been shown originally in the fly embryonic ventral nerve cord (Cleary and Doe, 2006; Doe, 2017) and subsequently in the fly visual system (Erclik et al., 2017; Li et al., 2013b) and mammalian neocortex (Oberst et al., 2019; Telley et al., 2016). Second, the combination of spatially restricted expression of cell fate determinants and temporal competence windows creates neuronal diversity by confining the generation of specific subtypes of neurons to specific neurogenic zones at different times. Elegant examples of such combinatorial diversification have recently been reported for both the fly visual system and the mammalian neocortex (Apitz and Salecker, 2018; Erclik et al., 2017; Mayer et al., 2018; Mi et al., 2018; Mora et al., 2018; Nowakowski et al., 2017; Quan et al., 2016). Third, in *Drosophila*, ample evidence demonstrates that individual neural progenitors can give rise to differentially fate-restricted daughters while also maintaining their own progenitor status through a binary cell fate choice mechanism mediated by the highly conserved Notch signaling pathway (Endo et al., 2007; Wheeler et al., 2008). In both the mammalian neocortex (Bonnefont et al., 2019; Castro et al., 2006; Imayoshi et al., 2010) and the cerebellum (Machold et al., 2007), there is evidence that Notch activity is required to maintain progenitors in a bi-potential state by preventing their differentiation. In this scenario, Notch signaling contributes to the temporal axis of neuronal diversity by maintaining progenitors as they pass through consecutive fate competence windows. In contrast, there is currently no evidence that common progenitors use Notch signaling to generate neuronal diversity in the mammalian brain through a binary cell fate

This is an open access article under the CC BY-NC-ND license (http://creativecommons.org/licenses/by-nc-nd/4.0/).

choice mechanism, leading to speculation that this aspect of neurogenesis is regulated differently in invertebrates and mammals.

The cerebellum is a hub for control of motor function and contributes to a number of higher brain functions, such as reward-related cognitive processes (Carta et al., 2019; Kostadinov et al., 2019; Wagner and Luo, 2020). Deficits in cerebellar development lead to severe neurological disorders, such as cerebellar ataxias (Manto et al., 2020) and medulloblastomas (Northcott et al., 2019), a heterogeneous and severe group of childhood brain tumors. Thus, it is important to understand the underlying cellular and molecular mechanisms controlling cerebellar development. Until recently, the consensus view of the development of the cerebellum (Leto et al., 2016) suggested that different types of cerebellar neurons arise at different time points from two spatially distinct progenitor pools located in a continuum along the fourth ventricle, either dorsally in the rhombic lip (RL) or ventrally in the ventricular zone (VZ). Two basic helix-loop-helix (bHLH) transcription factors called Atonal homolog 1 (Atoh1; RL) and Pancreas transcription factor 1 alpha (Ptf1a; VZ) mark these progenitor domains (Figure S1A) (Volpe et al., 2017; Wang and Zoghbi, 2001). During embryonic development, Atoh1$^+$ RL precursors give rise to glutamatergic neurons, while Ptf1a$^+$ VZ precursors give rise to GABAergic neurons (Leto et al., 2016).

Despite what appear to be independent spatial and temporal origins, several intriguing observations suggest that these precursors may share some common features. First, the cell fate in the two germinal niches can be switched when Atoh1 and Ptf1a are ectopically expressed in the VZ and RL, respectively (Wang et al., 2005; Yamada et al., 2014). Second, pseudo-time trajectory analysis of single-cell RNA sequencing (scRNA-seq) embryonic mouse cerebellum data suggests that a common pool of progenitors branches into either a glutamatergic fate or a GABAergic fate (Vladoiu et al., 2019). Third, the classic neural stem cell marker Sox2 is known as an early VZ marker (Pibiri et al., 2016). Cells expressing both Sox2 and the glutamatergic RL fate determinant Atoh1 have been observed in human cerebellar organoids (Muguruma et al., 2015), suggesting that Sox2$^+$ progenitors exist in both germinal zones. Very recent fate mapping of Sox2$^+$ progenitors in the RL has shown that they can give rise to excitatory neurons (Selvadurai et al., 2020).

The fact that Sox2$^+$ cells can give rise to both excitatory and inhibitory lineages is not inconsistent with the current consensus view of spatial and temporal segregation of progenitor domains (Leto et al., 2016). However, the studies highlighted above can also be interpreted to suggest that at least a subset of these Sox2$^+$ cells are in fact bi-potential embryonic cerebellar progenitors (ECPs), each of which can simultaneously generate both excitatory and inhibitory lineages. Whether such ECPs exist and how a binary excitatory versus inhibitory fate decision is regulated are unknown. Here we use sparse fate mapping and loss and gain of function (GOF) of Notch approaches in the mouse cerebellum and human cerebellar organoids, and we demonstrate that excitatory and inhibitory lineages can derive from common progenitors and that Notch activity is required for this decision.

RESULTS

GABAergic and glutamatergic neurons are generated simultaneously from the Sox2$^+$ progenitor pool

To identify markers for potential ECPs, we examined gene expression in the embryonic cerebellum in the Allen Brain Atlas for well-established neural progenitor markers known to be expressed at various stages of cerebellar development (Figure S1C), namely, Sox2 (Ahlfeld et al., 2017; Kelberman et al., 2008; Pibiri et al., 2016; Selvadurai et al., 2020), Nestin (Andreotti et al., 2018; Li et al., 2013a; Wojcinski et al., 2017), glutamate astrocyte-specific transporter (GLAST) (Bauer et al., 2012; Miyazaki et al., 2017; Yamada et al., 2000), S100β (Hachem et al., 2007; Landry et al., 1989), and glial fibrillary acidic protein (GFAP) (Vong et al., 2015; Wen et al., 2013; Yang et al., 2008). We found that both Sox2 and Nestin are highly expressed in both VZ and RL during early cerebellar neurogenesis, although Nestin expression appeared to be more sparse, consistent with previous fate mapping work showing the Nestin-expressing progenitors principally give rise to late-born interneurons and glial cells (Fleming et al., 2013; Wojcinski et al., 2017). We retrieved and analyzed a scRNA-seq dataset (ENA: PRJEB23051 dataset) (Carter et al., 2018) and found ~2,000 cells expressing Sox2, of which only 50% express Nestin (Figures S1D and S1E). Together with its more abundant expression in the tissue, this suggests that Sox2 is the best candidate for finding bi-potential ECPs capable of giving rise to both excitatory and inhibitory lineages. We verified this with antibody staining and found the Sox2 protein to be broadly expressed throughout the cerebellar anlagen (embryonic day [E] 9.5–E16; Figures S1F–S1J). Furthermore, some Sox2$^+$ cells express Atoh1, which is expressed in the cerebellar primordium as early as E9.5 (Figures S1F'–S1J').

The cerebellar cortex is composed of a well-defined limited number of cell types with characteristic locations and morphologies (Figures S1B and S2A). To begin testing the pluripotency of Sox2$^+$ progenitors, we performed lineage tracing by using *Sox2^{CreERT2}/Gt(ROSA)26Sor^{tdTomato}/Atoh1^{GFP}* pregnant mice injected with very low doses of tamoxifen (TM) at early embryonic stages (E11.5) and examined the adult cerebellum at postnatal day (P) 21. Consistent with the presence of bi-potential progenitors, we recovered most known cerebellar cortex neuronal and glial cell types in all the known layers (Figures S2B–S2H').

In the mammalian cerebellum, Purkinje cells (PCs) and granule cells (GCs) are the major GABAergic and glutamatergic neurons (Hibi and Shimizu, 2012; Wang and Zoghbi, 2001). PCs are born during E10.5–E13, but do not express the classical postmitotic marker Calbindin until E14.5 (Goldowitz et al., 1997; Morales and Hatten, 2006). Pax6 is a marker for GCs that is highly expressed in the RL at E11.5, and its strong expression can be observed in both outer and inner external granular layer (EGL) until the postnatal stages (Divya et al., 2016). Focusing on GCs and PCs, we repeated the lineage-tracing experiments lowering the TM dose to 0.03 mg at E10.5, the lowest dose that we found to reliably induce recombination in our mice, and examined the cerebellar cortex at P21 using Pax6 and Calbindin, respectively. We recovered both GCs and PCs in our clones (Figures 1A–1D), as well as inhibitory interneurons labeled with Pax2 (Figures 1E–1G''). Furthermore, at E15 we find that the progeny of Sox2$^+$

CellPress
OPEN ACCESS

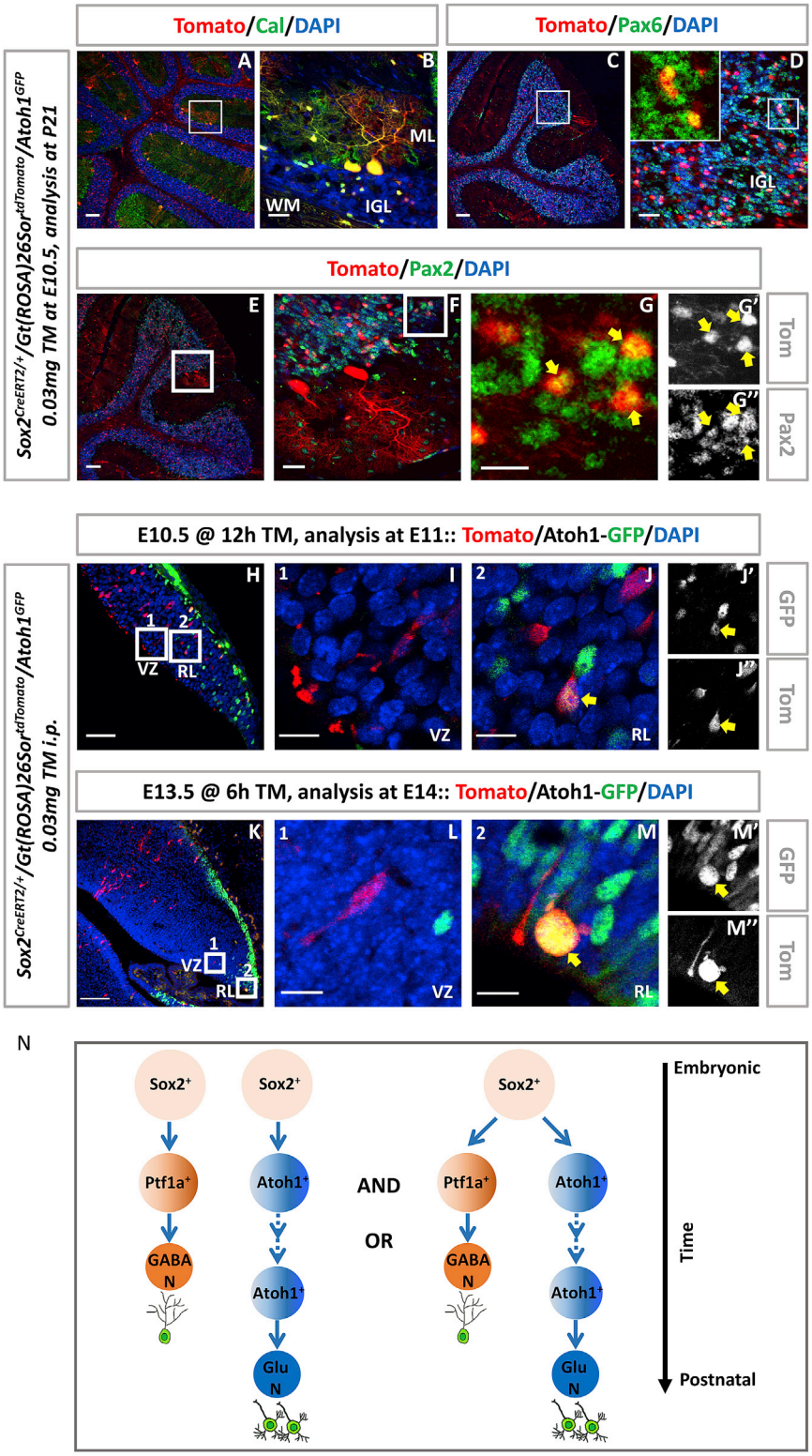

Figure 1. GABAergic and glutamatergic lineages are generated simultaneously from Sox2$^+$ progenitors

(A and C) Co-localization of tdTomato (red) with the PC marker Calbindin (Cal, green, A) or the GC marker Pax6 (green, C) in mouse cerebellum at P21. Scale bars: 100 μm.

(B and D) High magnification of the rectangular regions in (A) and (C). Scale bars: 25 μm.

(E and F) Co-localization of the IN marker Pax2 (green) and tdTomato (red) in the mouse cerebellum at P21. Scale bars: 100 μm and 25 μm.

(G–G'') Higher magnification of the rectangular region in (F). Scale bars: 25 μm.

(H) Lineage tracing of Sox2$^+$ cells (labeled by tdTomato, red) at E11 at 12 h after injection of 0.03 mg tamoxifen. Scale bars: 50 μm.

(I–J'') High magnification of the rectangular regions in (H), which show the tdTomato expression in the VZ (I) and RL (J–J''), respectively. Scale bars: 10 μm.

(K) Lineage tracing of Sox2$^+$ cells (labeled by tdTomato, red) at E14 at 6 h after injection of 0.03 mg tamoxifen. Scale bars: 100 μm.

(L–M'') High magnification of the rectangular regions in (K), which show the tdTomato expression in the VZ (L) and RL (M–M''), respectively. Scale bars: 15 μm.

(N) Schematic of the two hypotheses of how Sox2$^+$ progenitors generate both GABAergic and glutamatergic lineages in mouse cerebellum.

Yellow arrows indicate Pax2$^+$/Tomato$^+$ double-positive cells (G–G'') or Sox2$^+$/Atoh1-GFP$^+$ double-positive cells (J–J'' and M–M''). Nuclei were stained with DAPI (blue).

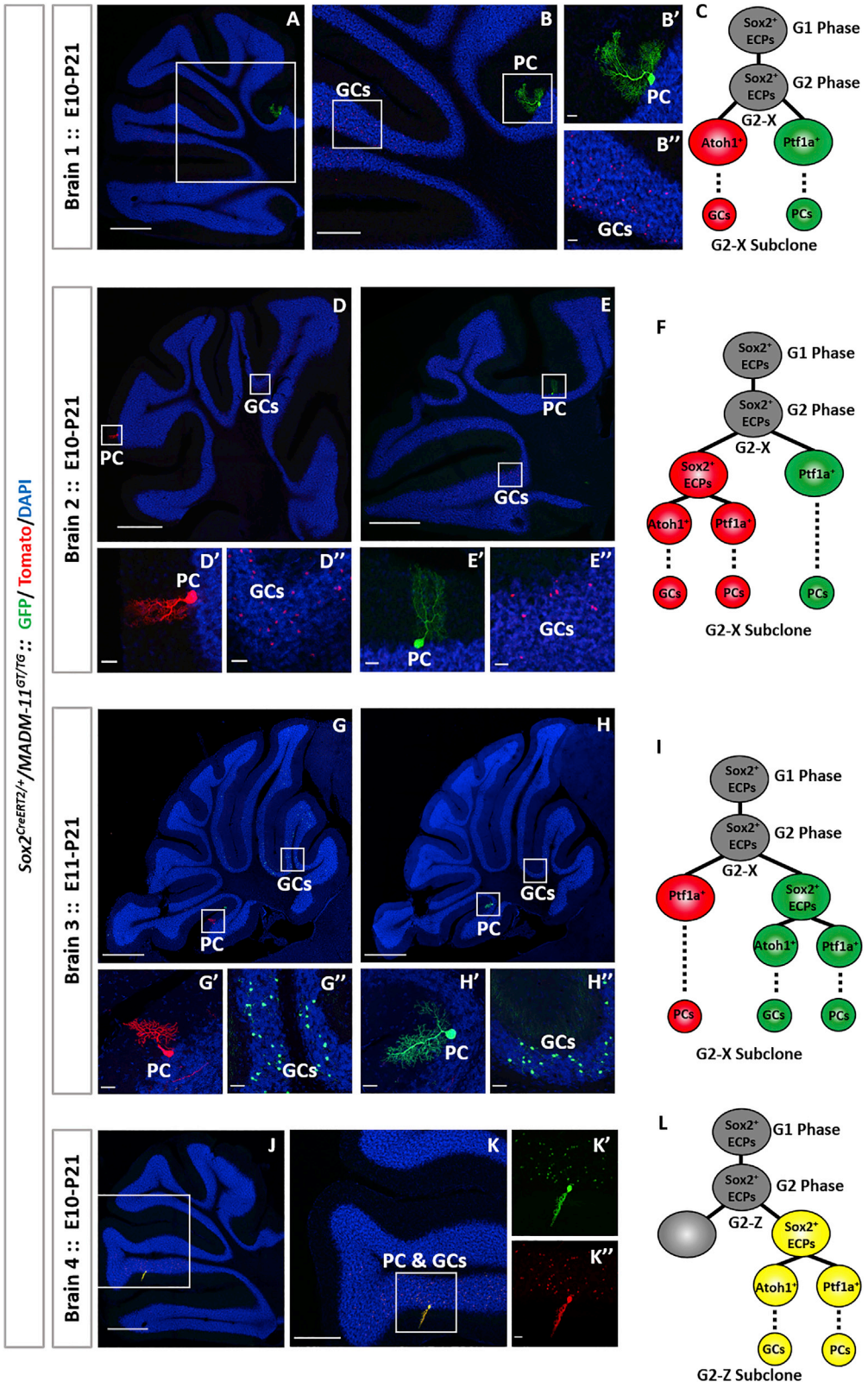

(legend on next page)

progenitors include all the known precursor cell types, as judged by their respective markers: Calbindin for nascent PCs (Figures S2I and S2J), Atoh1 and Pax6 (for excitatory precursors; Figures S2K and S2L), and Pax2 (for precursors of GABAergic interneurons; Figures S2M–S2O''). Glutamatergic deep cerebellar nuclei (DCNs) are produced in the RL at E10.5–E12.5 and migrate rostrally in a subpial stream (SPS) to enter the nuclear transitory zone (NTZ) (Fink et al., 2006). Olig2 is a marker for all DCN projection neurons, while Tbr1 and Pax6 are specific markers for glu-DCN neurons (Fink et al., 2006; Ju et al., 2016). Immunostaining results showed that Olig2$^+$, Pax6$^+$, and Tbr1$^+$ cells all co-localized with Tomato$^+$ cells at E15 (Figures S2P–S2V).

The scRNA-seq data suggested that relatively few Sox2$^+$ cells persist as late as ~E13. To increase the sparseness of our clones and examine them as soon as possible after the first cell division, we injected 0.03 mg of TM at both at E10.5 and E13.5 and examined embryos 12 or 6 h later to ensure we focus on the immediate progeny of the labeled progenitors. As expected, with a low TM dose and a short time induction, the combination resulted in rare labeled cells both at RL and VZ at E11 (Figures 1H–1J'') and even fewer labeled cells at E14 (Figures 1K–1M''). Surprisingly, however, these cells distributed equally between the RL and the VZ, strongly suggesting that precursors of the two lineages are generated simultaneously. Although the nature of this lineage-tracing approach cannot exclude the possibility that these very sparse clones derive from separate fate-restricted progenitors that divide simultaneously, the fact that we observe both PC and GC lineages within 6 h of sparse labeling does suggest the existence of bi-potential progenitors even as late as E13.5 that divide and simultaneously give rise to both inhibitory and excitatory cells in the cerebellar primordium (Figure 1N).

GABAergic and glutamatergic neurons are generated from single Sox2$^+$ ECPs

To investigate whether such bi-potent progenitors exist, we asked whether a single Sox2$^+$ ECP can generate PCs and GCs *in vivo*. To this end, we turned to the clonal mosaic analysis with double markers (MADM) technology (Beattie et al., 2017; Gao et al., 2014; Zong et al., 2005). MADM allows the tracing of the progeny of single progenitors by virtue of the mode of segregation of two different markers (one green and one red) that cannot be expressed except following Cre-induced recombination during the G2 phase of the cell cycle.

If the two markers segregate to two different daughter cells, in what is called the G2-X event (Figure S3A), the progeny of the two daughters will be labeled in two different colors within the same brain. In our case, if G2-X recombination occurs in a progenitor that will give rise to one Atoh1$^+$ daughter and one Ptf1a$^+$ daughter and both survive, this will create clones containing both PCs and GCs labeled in distinct colors (for example, green GCs and red PCs). If G2-X recombination occurs in a self-renewing ECP that itself will give rise to a bi-potential ECP, which will then divide again to give rise to one Atoh1$^+$ daughter and one Ptf1a$^+$ daughter and both survive, this will create clones containing both PCs and GCs labeled in the same color (e.g., green GCs and green PCs). Any and all clones meeting the conditions described above are direct and conclusive evidence for the existence of a common progenitor for the two lineages. Conversely, clones that contain only one cell type suggest that recombination occurred in a fate-restricted progenitor.

Alternatively, if the two markers segregate together, in what is called the G2-Z event (Figure S3B), then one daughter and its progeny will be labeled in yellow and the other will not be labeled at all and thus will not be detectable. In our case, if G2-Z recombination occurs in a self-renewing ECP that itself will give rise to a bi-potential ECP that will then divide again to give rise to one Atoh1$^+$ daughter and one Ptf1a$^+$ daughter and both survive, this will create clones containing both PCs and GCs labeled in yellow. Any yellow clones containing both PCs and GCs also provide conclusive direct evidence for a bi-potential progenitor for the two lineages. Single-cell-type yellow clones (for example, yellow GCs and unlabeled PCs) are consistent with, but do not demonstrate the existence of, bi-potential progenitors. In summary, any and all clones that contain both cell types in yellow, both cell types in red or green, or one cell type in red and the other in green conclusively demonstrate a common cell of origin for GCs and PCs.

We performed MADM in cerebellar Sox2$^+$ cells at both E10 and E11 and analyzed samples for GC and/or PC clones at P21. Consistent with sparsity of MADM clones (Beattie et al., 2017; Gao et al., 2014), we obtained 0.42 MADM event per brain hemisphere when injecting TM at E10 (32 clones in 76 brain hemispheres; Table S1) and 0.27 event when injecting TM 1 day later (23 clones in 86 brain hemispheres; Table S1). In 9 of the 55 clones (16.36%), we obtained both GCs and PCs in the same brain, with 6 clones being products of G2-X events and the remaining 3 products of G2-Z events with both PCs

Figure 2. Sparse MADM-based lineage tracing of individual ECPs in mouse cerebellum

(A) Single-progenitor G2-X-MADM clone at P21. One green PC and tens of red GCs were found in the same cerebellum. Scale bar: 500 μm.
(B) Higher magnification of the rectangular regions in (A). Scale bar: 250 μm. (B' and B'') Higher magnification of the rectangular regions in (B). Scale bars: 25 μm.
(C) Scheme of a single G2-X-MADM clone generated both fate-restricted red (GCs) and green (PCs) lineages.
(D and E) Single progenitor G2-X-MADM clone at P21. One red PC (D) and one green PC (E) and tens of red GCs were found in the same cerebellum. Scale bars: 500 μm. (D'–E'') Higher magnification of the rectangular regions in (D) and (E). Scale bars: 25 μm.
(F) Scheme of a single G2-X-MADM clone generated a green fate-restricted daughter cell (PCs lineage) and a red multipotent progenitor cell.
(G and H) Single progenitor G2-X-MADM clone at P21. One red PC (G) and one green PC (H) and tens of green GCs were found in the same cerebellum. Scale bars: 500 μm. (G'–H'') Higher magnification of the rectangular regions in (G) and (H). Scale bars: 25 μm.
(I) Scheme of a single G2-X-MADM clone generated a red fate-restricted daughter cell (PCs lineage) and a green multipotent progenitor cell.
(J) Single progenitor G2-Z-MADM clones at P21. One yellow PC and tens of yellow GCs were found in the same cerebellum. Scale bar: 500 μm.
(K) Higher magnification of the rectangular regions in (J). Scale bar: 250 μm. (K' and K'') Higher magnification of the rectangular regions in (K). Scale bars: 25 μm.
(L) Scheme of a single G2-Z-MADM clone generated a yellow bi-potential progenitor cell and the other one without labeling.
Nuclei were stained with DAPI (blue).

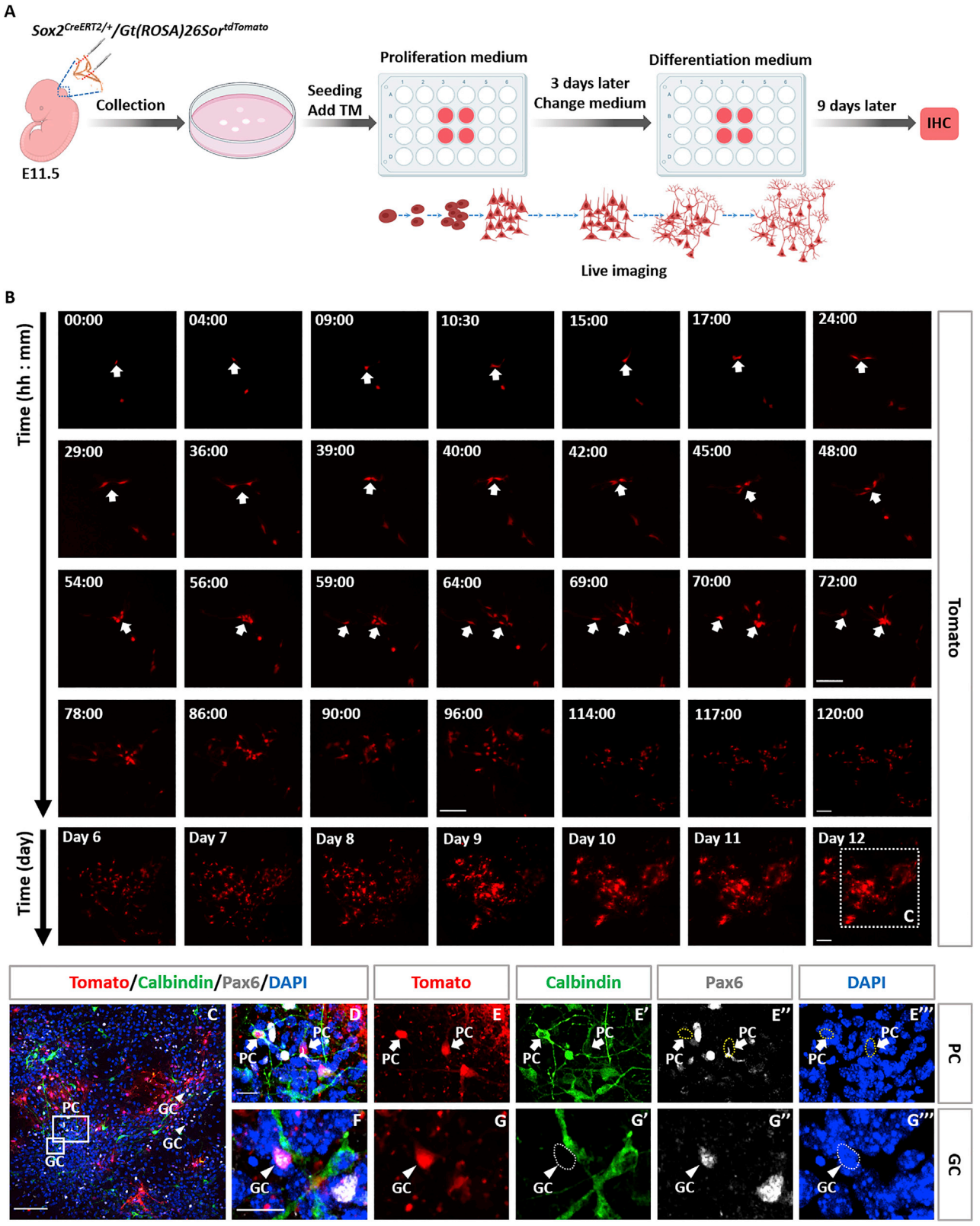

(legend on next page)

and GCs labeled in yellow (Table S1; Figures 2J–2L). Among G2-X clones, we obtained two scenarios: (1) G2-X recombination occurred in progenitors that generated two fate-restricted daughter cells such that at P21 we obtained red-labeled GCs and green-labeled PCs in the same clone (Figures 2A–2C); and (2) G2-X recombination occurred in self-renewing progenitors that generated one bi-potential ECP, which then generated same-color-labeled PCs and GCs (i.e., either both in green or both in red), and another fate-restricted Ptf1a$^+$ cell that generated fate-restricted GABAergic lineage in the other color (Figures 2D–2I). These 9 clones that contained both PCs and GCs provide direct conclusive evidence that excitatory and inhibitory neurons can derive from a single bi-potent common progenitor.

In addition, we obtained yellow clones containing either GCs only (8 clones, 14.55%) or PCs only (11 clones, 20%), consistent with a G2-Z event in a single progenitor cell (Figures S3C–S3E''' and S3K–S3L'; Table S1). In all of our single progenitor clones, we observed a much larger number of GCs than PCs, consistent with the transient amplification of GC precursors prior to neurogenesis (Espinosa and Luo, 2008). Finally, we also obtained (10/55, 18.18%) green and red single PC clones (Table S1; Figures S3F and S3G) indicating recombination occurred in Sox2$^+$ cells that had already committed to a specific Ptf1a$^+$ lineage and also (17/55, 30.91%) green or red single-cell-type clones (Table S1; Figures S3H–S3J') (Ahlfeld et al., 2017; Kelberman et al., 2008; Pibiri et al., 2016; Selvadurai et al., 2020).

Single Sox2$^+$ ECPs have an intrinsic potential to generate both PCs and GCs

To test whether Sox2$^+$ ECPs are intrinsically bi-potential, we carried out *in vitro* primary culture of cerebellar progenitors. We harvested ECPs from *Sox2^{CreERT2}/Gt(ROSA)26Sor^{tdTomato}* E11.5 embryos, sparsely labeled subsets of them by adding TM to the culture, and performed time-lapse video microscopy for 12 consecutive days to trace the fate of individual Sox2$^+$ ECPs (Figure 3A). Cells were kept under proliferative conditions for the first 3 days of culture to allow clonal expansion of single Sox2$^+$ ECPs, followed by switching to a pro-differentiation medium for another 9 days to induce the production of both granule and Purkinje neurons (Kawasaki et al., 2000; Su et al., 2006). We traced the formation of 39 clones and found that 12 of them (31%) contained both PCs (Calbindin$^+$/Tomato$^+$) and GCs (Pax6$^+$/Tomato$^+$) derived from the same progenitor (Figures 3B–3G'''; Videos S1 and S2). These data demonstrate that a single Sox2$^+$ ECP has an intrinsic ability to generate both inhibitory and excitatory neurons.

Finally, we asked whether a common origin of GCs and PCs is conserved in human. We generated human induced pluripotent stem cell (iPSC)-derived cerebellar organoids using a previously described protocol (Ishida et al., 2016; Muguruma et al., 2015). In order to sparsely label early Sox2$^+$ human ECPs, we electroporated pGL3-Sox2Cre and pCAG PiggyBac (Pbase) and pPBCAG-LSL-Venus vectors into cerebellar organoids at 25 days (Figures S3M–S3N''' and S3S). At day 35 the cerebellar organoids expressed several markers, such as Ptf1a, Atoh1, Skor2, and Pax6 (Ballabio et al., 2020a; Muguruma et al., 2015), but only from days 38 to 41 were we able to detect Calbindin$^+$ cells. Therefore, we traced the Sox2$^+$ ECPs fate at 41 days of organoid culture (Figure S3S). In all organoids, we observed both PCs (Venus$^+$/Calbindin$^+$; Figures S3O–S3P''') and GCs (Venus$^+$/Pax6$^+$; Figures S3Q–S3R''').

In summary, our data thus far provide direct evidence for the existence of Sox2$^+$ ECPs capable of generating both GABAergic and glutamatergic lineages.

Differential expression of Notch pathway genes in different ECPs

To identify the molecular underpinnings of the diversification of cerebellar neurons from common progenitors, we first analyzed available scRNA-seq data to define the molecular features of different cerebellar cell types during early stages. We retrieved the original data from E10–E13 (ENA: PRJEB23051 dataset) (Carter et al., 2018) and used the Chromium system (10x Genomics) to profile the populations of each individual developmental time point. Based on known cerebellar markers and transcriptional similarity, we identified individual clusters and mapped pseudo-time trajectory for cerebellar lineages (Figures 4A–4D). This confirmed that Sox2$^+$ progenitors can give rise to two major lineages: glutamatergic cells from RL and GABAergic cells from VZ (Figure 4A). Previous work manipulating Notch1 function throughout the cerebellar anlagen identified a requirement for Notch1 in the maintenance of RL progenitors by acting as an antagonist of RL-derived neurogenesis through the suppression of Atoh1 expression (Machold et al., 2007). We asked whether the role of Notch signaling in Sox2$^+$ ECPs is only to contribute to the temporal axis of neurogenesis by maintaining progenitor fate, as its classic role in mammalian neurogenesis, or whether it is also involved in the binary excitatory versus inhibitory cell fate decision. During canonical Notch-dependent binary cell fate decisions, cells interact to adopt mutually exclusive "opposing" terminal fates (Artavanis-Tsakonas et al., 1999). We therefore began by testing whether the expression of Notch pathway genes correlates with cell fate in the scRNA-seq data. We identified individual clusters for Notch signaling-related genes and found that canonical Notch target genes Hes5 and Hes1 are highly expressed in Ptf1a$^+$ and

Figure 3. GABAergic and glutamatergic lineages are generated from single Sox2$^+$ progenitor *in vitro*

(A) Schematic representation of the mouse cerebellar progenitors primary culture for cell proliferation and differentiation.

(B) Time-lapse video recording showed that a single Sox2 progenitor cell (Tomato$^+$, red) could divide several times to generate a cluster. Arrows indicate the Tomato$^+$ cells that we focused on.

(C) Immunolabeling of both PC marker (Calbindin, green) or GC marker (Pax6, gray) co-localized with Tomato (red) 9 days after cell differentiation, respectively. Arrowheads indicate Pax6$^+$/Tomato$^+$ double-positive cells.

(D–G''') Higher magnification of the rectangular region in (C). Arrows indicate Calbindin$^+$/Tomato$^+$ double-positive cells, and arrowheads indicate Pax6$^+$/Tomato$^+$ double-positive cells.

Nuclei were stained with DAPI (blue). Scale bars: 100 μm and 15 μm.

Sox2$^+$ cells when compared with Atoh1$^+$ cells, at both E12 and E13 (Figures 4E–4H). We next examined the expression of Notch1 and 5 of its ligands in these three populations (Table S2). We found that ECPs (green) express high levels of the Notch1, Hes1, and Hes5 mRNAs but very low levels of the ligands Dll1 and Dll3 (Figures 4I–4R). Ptf1a$^+$ inhibitory precursors (red) express Notch1, Hes1, and Hes5 to a lesser extent than ECPs, but much higher levels of the *trans*-activating ligand Dll1 and slightly higher levels of the *cis*-inhibiting ligand Dll3 (Ladi et al., 2005) (Figures 4I–4R). Atoh1$^+$ excitatory precursors (blue) express the lowest levels of the Notch1 receptor but the highest levels of the ligands, especially Dll3 (Figures 4I–4R). Taken together, analysis of Notch signaling-related genes in these three populations revealed that Sox2$^+$ ECPs have the highest level of Notch activity, followed by Ptf1a$^+$ inhibitory precursors, with Atoh1$^+$ excitatory precursors having the lowest levels of Notch activity but the highest levels of Notch ligands. These observations suggest that Notch activity segregates the three populations from each other: first the bi-potential ECPs from their fate-restricted Ptf1a$^+$ and Atoh1$^+$ daughters and then Ptf1a$^+$ inhibitory precursors from Atoh1$^+$ excitatory precursors. We set out to test this idea by manipulating Notch activity specifically within Sox2$^+$ ECPs.

Notch1 regulates inhibitory versus excitatory precursor fate decision in Sox2$^+$ ECPs

First, we asked whether the choice between Ptf1a$^+$ and Atoh1$^+$ cells requires Notch signaling. We examined Notch1 loss of function (LOF) either in clones using *Sox2^{CreERT2}/Notch1^{flox}/Atoh1^{GFP}* conditional knockout (cKO) mice (Figures S4A–S4E) or in Presenilin1 (Psn1) KO mice, which have a near-complete loss of Notch signaling activity (Figures S4F–S4H). Because of the mutual suppression of Ptf1a and Atoh1, the wild-type cerebellar precursors rarely co-express Atoh1 and Ptf1a (Yamada et al., 2014). However, bi-potential Sox2$^+$ ECPs may briefly express both fate potentials before a decision is made. If so, we might find a snapshot of this moment in their development in the scRNA-seq data. Examining these data at E10–E13, we did indeed find Sox2$^+$/Atoh1$^+$/Ptf1a$^+$ triple-positive cells, demonstrating the existence of individual bi-potential ECPs at the gene regulatory level. We found that these cells are very rare between E10 and E11, quickly peaking between E11 and E12 before dropping again between E12 and E13 (Figure 5A). The peak at E12 indicates that this is a critical time point for the fate choice of Sox2$^+$ ECPs; therefore, we examined Ptf1a and Atoh1 protein expression in Notch LOF conditions at E12. We found that in control ECP clones (Figures 5B–5D" and 5H) and control Psn1$^{+/-}$ mice (Figures 5I–5K" and 5O), the vast majority of committed precursors exclusively express either Ptf1a or Atoh1, with very few cells expressing detectable levels of both markers. In contrast, in Notch1$^{-/-}$ clones (Figures 5E–5H) and in Psn1 KO mice (Figures 5L–5O), we observed a significant (~3.5-fold) increase in the number of double-positive precursors. Interestingly, most of these cells were found at the VZ/RL boundary extending into the VZ. Together with the lineage-tracing evidence, these data suggest that individual daughters of ECPs can adopt either an inhibitory or an excitatory fate, and that the decision between these two fates requires Notch signaling. If this is correct, perturbing Notch activity should perturb the ratio of inhibitory to excitatory precursors.

To test this, we quantified the numbers and ratios of Atoh1$^+$ and Ptf1a$^+$ cells under Notch1 LOF conditions. First, we quantified the number of Sox2$^+$ cells that also express Atoh1 and found a progressive increase in the number of these cells with the progressive reduction in number of Notch1 copies (Figures 6A–6D). Furthermore, ectopic Sox2$^+$/Atoh1$^+$ cells were found within the VZ, especially under Notch1$^{-/-}$ conditions (Figure 6C), indicating a possible conversion of inhibitory VZ precursors into excitatory precursors. To directly test whether this is the case, we quantified the relative abundance of Ptf1a$^+$ and Atoh1$^+$ cells and found that the increase in Atoh1$^+$ cells came at the expense of Ptf1a$^+$ cells, which were significantly decreased in Notch1$^{-/-}$ ECP clones (Figures 6G–6I), as well as Psn1 KO mice (Figures 6L–6N). We observed a similar change in the relative expression of Atoh1 and Ptf1a mRNAs (Figures 6E, 6F, 6J, 6K, S4N, and S4O). Importantly, the ratio of the increase in Atoh1$^+$ cells was nearly identical to the ratio of the decrease in Ptf1a$^+$ cells (0.672 versus 0.673; Figures 6I and 6N), further supporting a Notch-dependent common origin of the two precursors. To confirm that this is a reduction in inhibitory GABAergic precursors and not only in Ptf1a expression, we examined the expression of other VZ precursor markers, namely, Olig2, which maintains the identity of PC progenitors (Ju et al., 2016), and Lhx1/5, a marker for early GABAergic cells (Hori et al., 2008; Muguruma et al., 2015), in Psn1 KO mice and found that levels of Olig2 mRNA were also decreased (Figure S4P), as were the numbers of Olig2$^+$ and Lhx1/5$^+$ cells, concomitantly with the increase in the number of Atoh1$^+$ cells (Figures S4I–S4M). Importantly, these changes in cell fate were not accompanied by changes in the degree of proliferation or cell death (Figure S5). Therefore, Notch1 signaling regulates the choice between excitatory and inhibitory precursor fate. Finally, we asked whether Notch inhibition also suppresses GABAergic fate in human cerebellar organoids by treating differentiating organoids with the gamma-secretase inhibitor dibenzazepine (DBZ), which results in a strong inhibition of Notch signaling. This resulted in a strong increase of Atoh1 expression and reduction of both Ptf1a expression and Calbindin$^+$ cell number, indicating a loss of GABAergic PCs (Figures S6A–S6F).

Notch GOF in ECPs maintains their stem cell fate in cerebellar primordium

During cortical development, transient gain of Notch function results in progenitors skipping the production of early-born (deep layer) neurons and thus favoring the production of late-born (upper layer) cells. Consequently, the effect of Notch GOF is to maintain cells in progenitor state to contribute to the temporal axis of neuronal diversification. However, our data show that Sox2$^+$ ECPs generate inhibitory and excitatory lineages in the cerebellum simultaneously, and that the inhibitory versus excitatory binary fate choice requires Notch signaling. To better understand the role of Notch signaling in the balance between maintaining progenitors and regulating binary cell fate, we analyzed the effects of overexpression of the constitutively active Notch1 intracellular domain (NICD) on ECPs. We generated Notch1 GOF ECP clones using *Sox2$^{CreERT2/+}$/Gt(ROSA)*

CellPress
OPEN ACCESS

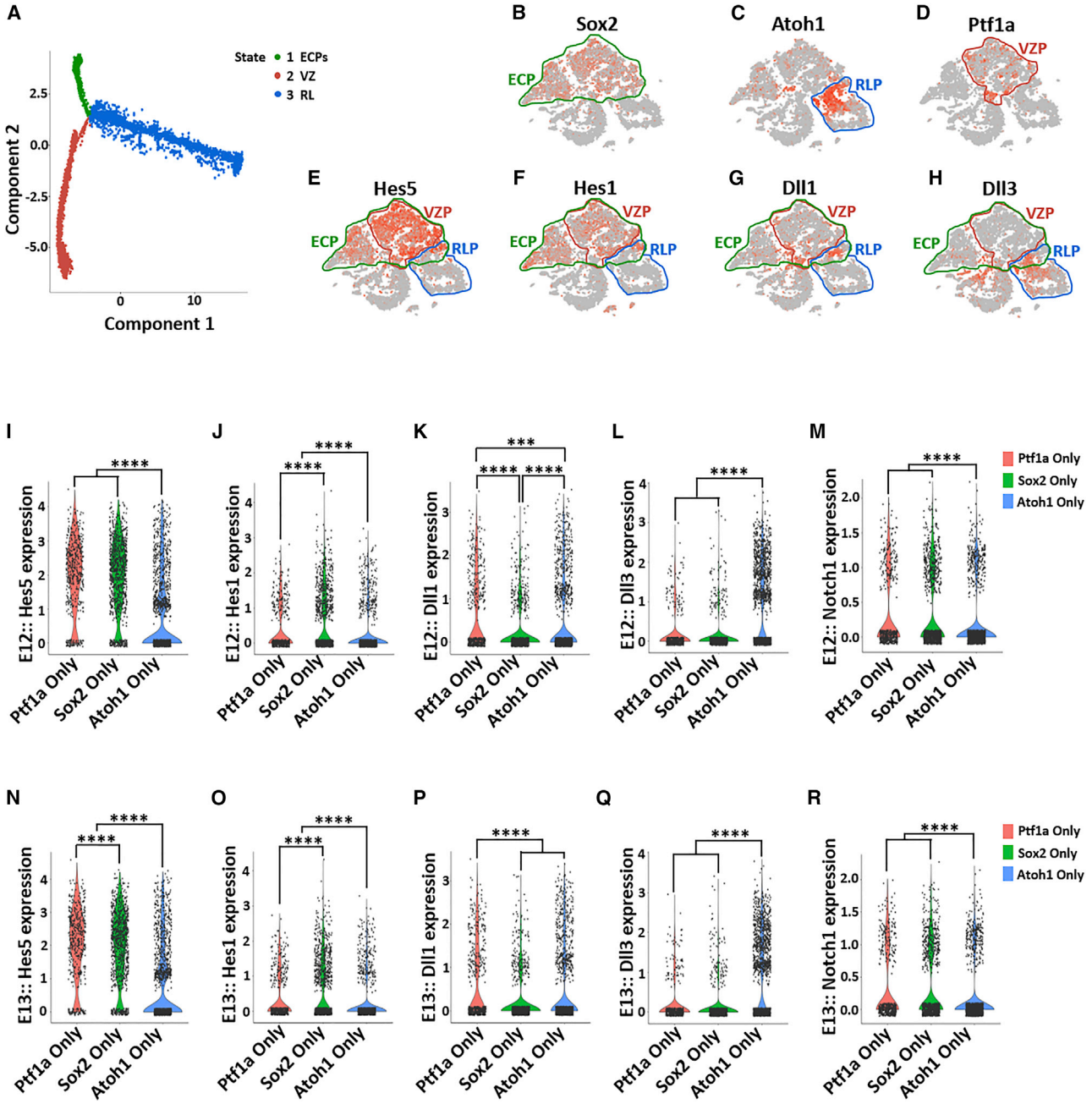

Figure 4. Analysis of Notch signaling gene expression in scRNA-seq data from embryonic cerebellar progenitors

(A) Pseudo-time trajectory of scRNA-seq data in the E10–E13 cerebellum: ECPs (green), VZ GABAergic lineages (red), and RL glutamatergic lineages (blue).

(B) t-SNE (t-distributed stochastic neighbor embedding) visualizations of cerebellar-derived cell clusters at E10–E13. Cells that express only Sox2 but neither Atoh1 nor Ptf1a are defined as ECPs (inside the green line).

(C and D) t-SNE shows cell-type-specific marker expression: Atoh1 and Ptf1a. Atoh1$^+$ clusters are rhombic lip progenitors (RLPs, inside the blue line) and Ptf1a$^+$ clusters are ventricular zone progenitors (VZPs, inside the red line). Cells were color coded according to gene expression with the cells expressing the gene indicated colored in orange-red.

(E–H) t-SNE showing the expression of Notch signaling genes: Hes5, Hes1, Dll1, and Dll3.

(I–R) Violin plot showed the expression of Hes5, Hes1, Dll1, Dll3, and Notch1 in three different groups: Ptf1a-only, Sox2-only, and Atoh1-only at both E12 (I–M) and E13 (N–R). ***$p < 0.001$, ****$p < 0.0001$, one-way ANOVA.

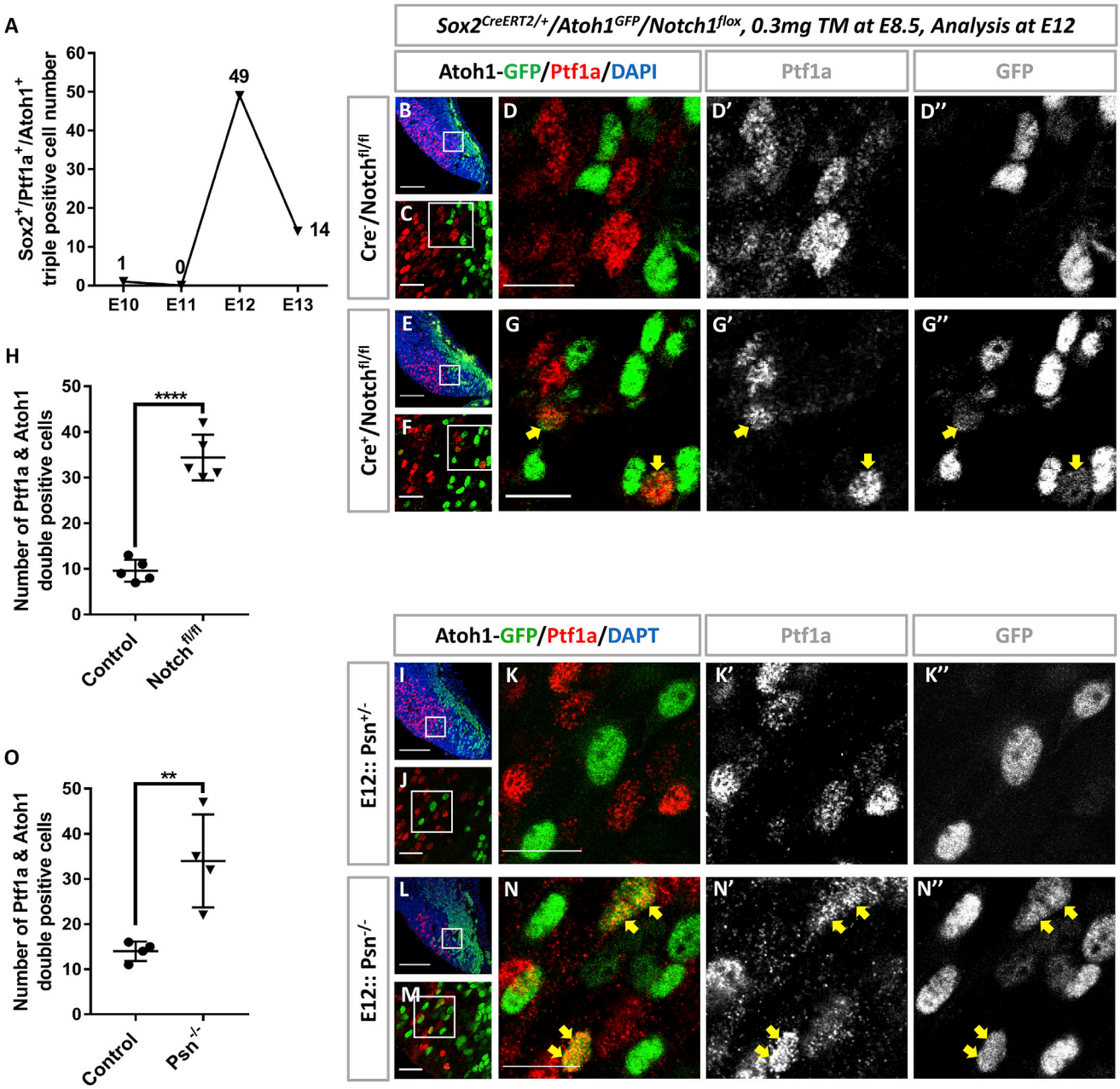

Figure 5. Notch loss of function increases Ptf1a and Atoh1 double-positive cells at the VZ-RL boundary

(A) Analysis of Sox2$^+$/Ptf1a$^+$/Atoh1$^+$ triple-positive cells in scRNA-seq data from embryonic cerebellar progenitors.

(B and C) Immunostaining for Ptf1a$^+$ (red) and Atoh1-GFP$^+$ (green) reveals very few double-positive cells at E12 in control cerebella. n = 5.

(D–D'') Higher magnification of the rectangular region in (C).

(E and F) Immunostaining for Ptf1a$^+$ (red) and Atoh1-GFP$^+$ (green) reveals increased double-positive cells at E12 in Notch1 cKO cerebellum. n = 5.

(G–G'') Higher magnification of the rectangular region in (F). Arrows indicate Ptf1a$^+$ and Atoh1-GFP$^+$ double-positive cells.

(H) Percentage of Ptf1a$^+$ and Atoh1-GFP$^+$ double-positive cells in control and Notch1 cKO cerebella.

(I and J) Immunostaining for Ptf1a$^+$ (red) and Atoh1-GFP$^+$ (green) double-positive cells at E12 in control cerebellum. n = 4.

(K–K'') Higher magnification of the rectangular region in (J).

(L and M) Immunostaining for Ptf1a$^+$ (red) and Atoh1-GFP$^+$ (green) double-positive cells at E12 in Psn KO cerebellum. n = 4.

(N–N'') Higher magnification of the rectangular region in (M).

(O) Percentage of Ptf1a$^+$ and Atoh1-GFP$^+$ double-positive cells in control and Psn KO cerebella. Arrows indicate Ptf1a$^+$ and Atoh1-GFP$^+$ double-positive cells. Nuclei were stained with DAPI (blue). Scale bars: 100 μm, 25 μm, and 15 μm. Data are presented as mean ± SD. **$p < 0.01$, ****$p < 0.0001$, t tests.

CellPress
OPEN ACCESS

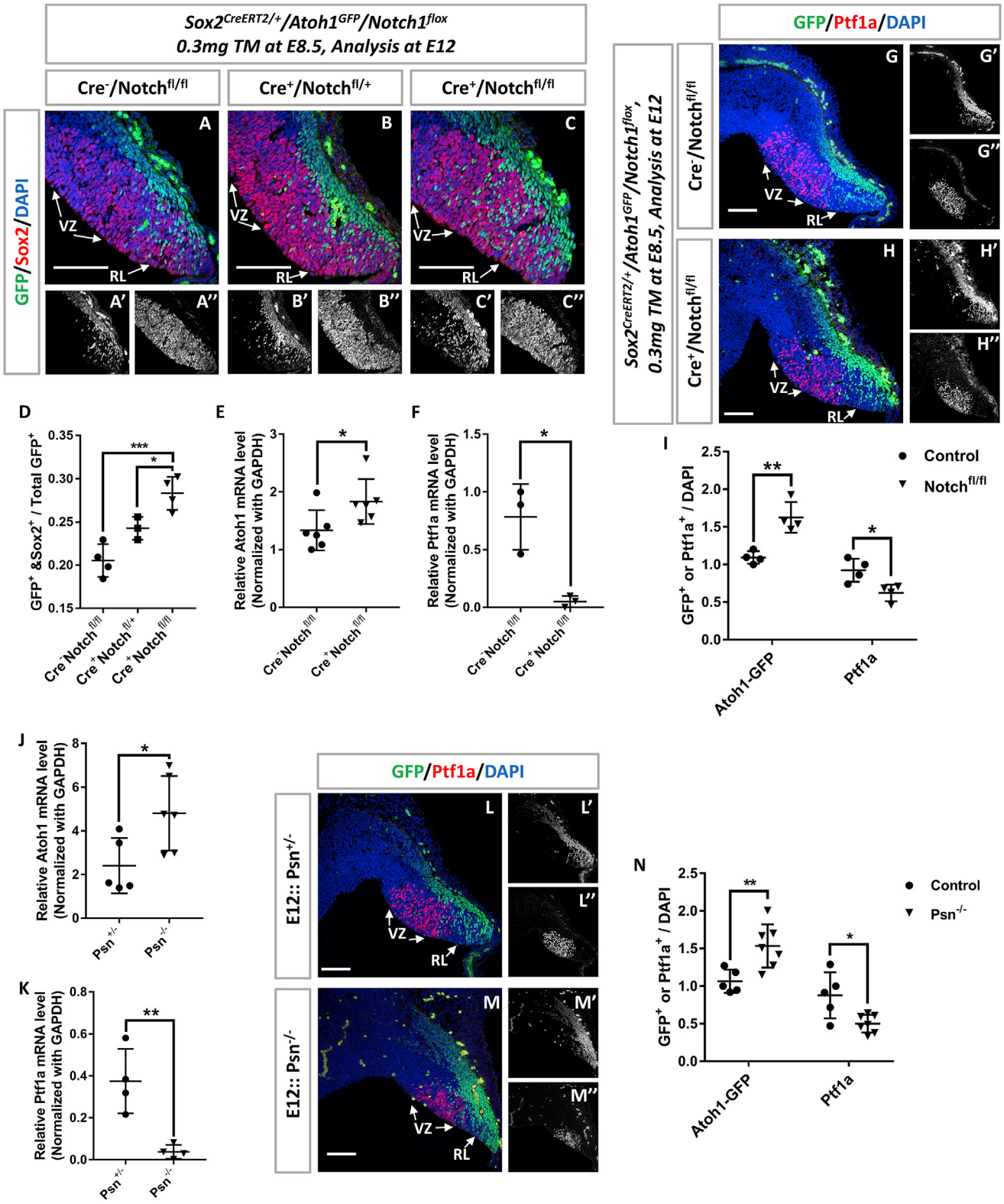

(legend on next page)

26Sor^{tdTomato}/*R26R*$^{stop\text{-}NICD\text{-}nGFP}$ mice and examined cell fate inside the clones at E12, when all three cell types (ECPs, VZPs, and RLPs) are abundant. We found that Notch GOF strongly reduces the number of both Ptf1a$^+$ and Atoh1$^+$ precursors (Figures 7A–7J, S6G–S6J'', and S6M). However, whereas we were able to detect Ptf1a$^+$ cells (Figures 7C–7D'' and S6G–S6H''), no Atoh1$^+$ cells were detected within the Notch1 GOF clones (Figures 7H–7I'' and S6I–S6J''). Quantification confirmed that the effect was significantly stronger on Atoh1$^+$ cells than on Ptf1a$^+$ cells (Figures 7K and S6M). Lastly, we checked Sox2 expression within the NICD-GFP clones and found that Notch GOF in progenitor cells significantly increased Sox2$^+$ cells in both the RL and the VZ (Figures 7L–7P, S6K–S6L'', and S6N) at the expense of Ptf1a$^+$ and Atoh1$^+$ cells. Importantly, the inhibition of differentiation induced by Notch GOF was long lasting (Figure S7). Almost all NICD-GFP$^+$ cells retained an undifferentiated state at E16 with very few NICD-GFP$^+$ cells differentiating into Calbindin$^+$ PCs (Figures S7A–S7C'') and none of the cells differentiating into Atoh1$^+$ GC precursors (Figures S7D–S7F''), while in both the RL and the VZ the NICD-GFP$^+$ cells retained high levels of Sox2 expression (Figures S7G–S7L). Altogether, our data demonstrate that Notch activity dictates cell fate in bi-potential cerebellar progenitor cells.

DISCUSSION

In this work we show that, in contrast with what is classically described, an appreciable proportion of GABAergic and glutamatergic neurons of the cerebellar cortex in both mouse and human organoids can indeed derive from common progenitors that we here term ECPs. Population and single-cell lineage-tracing approaches demonstrated that Sox2$^+$ ECPs cells are likely to give rise to multiple cerebellar cell types, including GABAergic and glutamatergic neurons, as well as astroglial cells. These progenitors span the RL and the VZ and are characterized by the expression of Sox2$^+$ and very high levels of Notch activity. This finding led us to ask how these common progenitors give rise to different types of neurons. Analysis of scRNA-seq data suggested cell fate diversification may be influenced by Notch signaling. This was surprising because although Notch activity is known to distinguish progenitors from differentiated daughters in all lineages where it was examined, no evidence for a role of Notch signaling in neuronal binary cells fate choice has been found in mammalian brain neurogenesis. Our *in vivo* genetic analyses using loss and gain of Notch1 function, as well as Psn1 KO mice, support a simple model whereby early common progenitors generate precursors that express different levels of the Notch ligands Delta1 and Delta3 and signal back to their mother cells and to each other to segregate into different cell fates. This creates a binary choice where different types of precursors eventually generate excitatory versus inhibitory cells, respectively. The expression of Delta3 largely by RL precursors allows these precursors to further repress Notch activity cell autonomously, because Delta3 is thought to act as a cell-autonomous *cis*-inhibitor of the Notch receptor (Ladi et al., 2005). We thus provide mechanistic evidence for how common progenitors can generate both excitatory and inhibitory lineages in the mammalian brain. It will be interesting to determine the developmental trajectory of mixed fate MADM clones and query the effects of Notch loss in such clones. It will be also interesting to test precisely how Notch activity in ECPs or their daughters plays a role in disorders of cell fate or stem cell behavior such as medulloblastomas, as recent work suggests (Ballabio et al., 2020b). The human organoid model presented here will allow future careful dissection of the similarities and differences between mouse and human cerebellar development at single-cell resolution. Finally, it will be interesting to determine how ECPs respond to niche signals possibly through transplantation experiments of labeled ECPs following lineage tracing.

It is very interesting to note that although PCs and GCs themselves are generated on very different temporal scales, with PCs born much earlier than GCs, many of their precursors are specified at the same time. GC production is late because GC precursors undergo several rounds of transient amplification before generating neurons, thus creating this pseudo-heterochrony. The transient amplification of GC precursors is driven by Atoh1, which itself regulates, and is regulated by, Notch signaling. Our work provides a developmental and molecular framework for how common progenitors can create cell-type diversity across different timescales through the highly conserved process of binary cell fate specification. In *Drosophila* neuronal lineages, the two daughter neurons of the same precursor use Notch to adopt different identities during terminal cell division (Artavanis-Tsakonas et al., 1999; Bhat, 2014; Pinto-Teixeira and Desplan, 2014). Similarly, spinal cord inhibitory interneurons use Notch activity to adopt different identities (Peng et al., 2007). Single-cell analysis in the neocortex is beginning to reveal significant diversity of excitatory neuronal fates in the same cortical layers (Pfeffer and Beltramo, 2017). It would be interesting to test whether Notch signaling also regulates the fate of cortical sister neurons where the lack of sufficient markers of neuronal diversity may have precluded such findings in the past.

Figure 6. Notch loss of function in cerebellar progenitors favors Atoh1$^+$ progenitors at the expense of Ptf1a$^+$ progenitors

(A–C'') Immunostaining for Sox2$^+$ (red) and Atoh1-GFP$^+$ (green) at E12 in Cre$^-$/Notch$^{fl/fl}$ (n = 4), Cre$^+$/Notch$^{fl/+}$ (n = 3), and Cre$^+$/Notch$^{fl/fl}$ (n = 4) mice.

(D) Percentage of Atoh1-GFP$^+$/Sox2$^+$ double-positive cells within all Atoh1-GFP$^+$ cells in the three genotypes. *$p < 0.05$; ***$p < 0.001$, one-way ANOVA.

(E and F) Comparison of Atoh1 (n = 6) and Ptf1a (n = 3) mRNA levels in Cre$^-$/Notch$^{fl/fl}$ and Cre$^+$/Notch$^{fl/fl}$ mice using RT-PCR at E12. *$p < 0.05$, t tests.

(G–H'') Immunostaining for Ptf1a$^+$ (red) and Atoh1-GFP$^+$ (green) at E12 in control cerebella (G–G'') and in Notch1 conditional KO (cKO) cerebella (H–H''). n = 4.

(I) Percentage of Ptf1a$^+$ cells or Atoh1-GFP$^+$ cells among all cells (DAPI, blue) in control and Notch1 cKO cerebellum. *$p < 0.05$; **$p < 0.01$, t tests.

(J and K) Comparison of Atoh1 (n = 5 for control group and n = 6 for Psn KO group) and Ptf1a (n = 4) mRNA levels in control and Psn KO cerebellum using RT-PCR at E12. *$p < 0.05$; **$p < 0.01$, t tests.

(L–M'') Immunostaining for Ptf1a$^+$ (red) and Atoh1-GFP$^+$ cells (green) at E12 in control (L–L'', n = 5) and Presenilin1 (Psn) KO cerebella (M–M'', n = 7).

(N) Percentage of Ptf1a$^+$ cells or Atoh1-GFP$^+$ cells within all cells (DAPI) in control and Psn KO cerebella. *$p < 0.05$; **$p < 0.01$, t tests.

Scale bars: 100 μm and 25 μm. Data are presented as mean ± SD.

CellPress
OPEN ACCESS

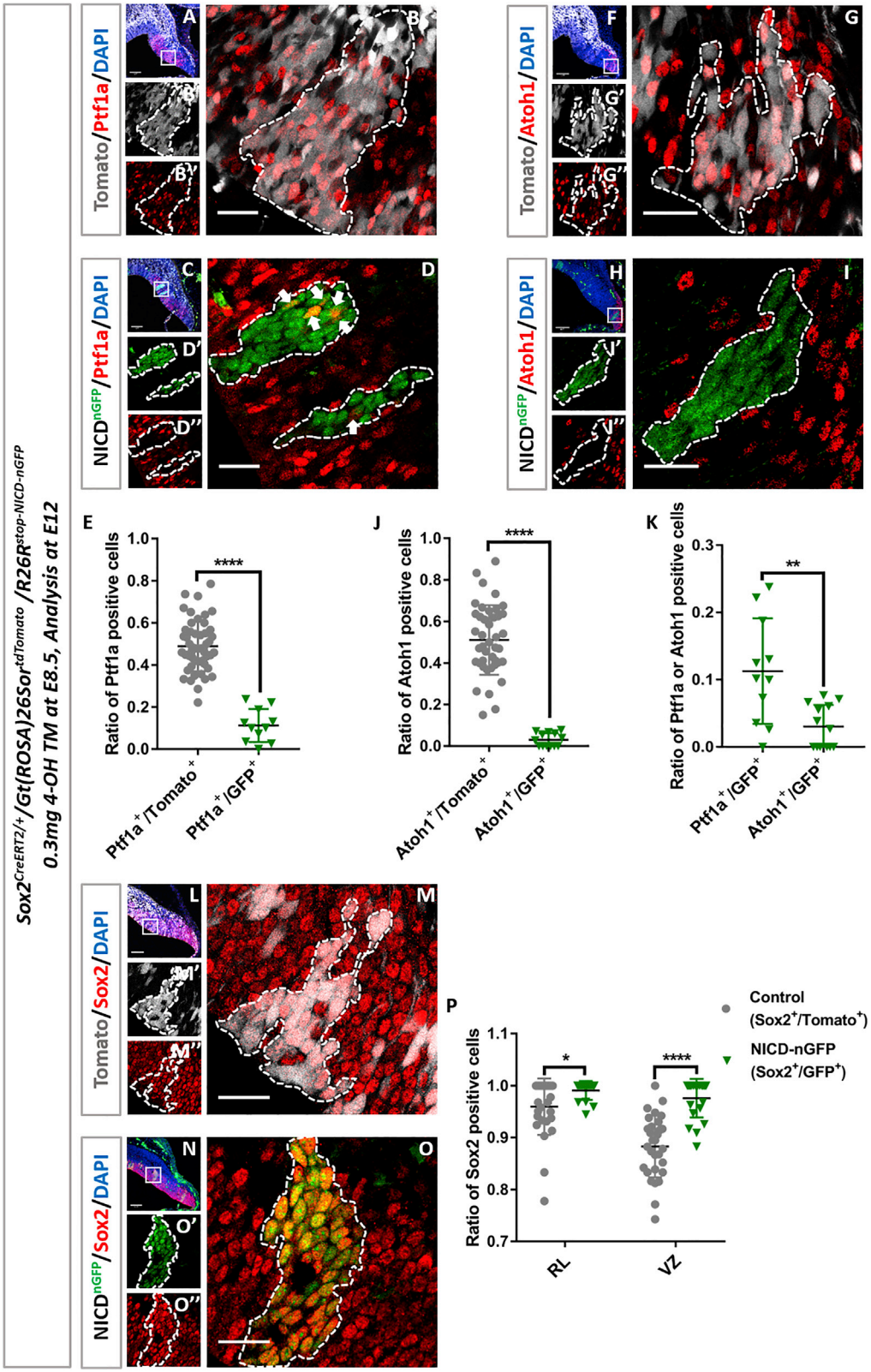

(legend on next page)

In *Drosophila*, part of the generation of cells with different Notch-dependent fates relies on asymmetric cell division of progenitors and the biased segregation of Notch inhibitors. Whether the production of Atoh1$^+$ and Ptf1a$^+$ cells is similarly modulated by asymmetric division of Sox2$^+$ progenitors needs further investigation. Because the bone morphogenetic proteins (BMPs) signaling and the diffusible mitogen Sonic hedgehog (Shh) signaling are also key regulators involved in GABAergic and glutamatergic lineage generation and differentiation (Fleming et al., 2013; Huang et al., 2010; Laudet et al., 1993; Machold et al., 2007), the integration between these activities and binary cell fate determination would be an interesting avenue of future work. Recent work suggests a common developmental basis for the evolution of cerebellar nuclei from conserved cell types (Kebschull et al., 2020). The derivation of at least some GCs and PCs from common progenitors via Notch-mediated binary cell fate choice suggests one possible genetic basis for how the excitatory-to-inhibitory ratio may change during evolution.

STAR★METHODS

Detailed methods are provided in the online version of this paper and include the following:

- KEY RESOURCES TABLE
- RESOURCE AVAILABILITY
  - Lead contact
  - Materials availability
  - Data and code availability
- EXPERIMENTAL MODEL AND SUBJECT DETAILS
  - Mice
  - Primary culture of mouse cerebellar progenitor cells
  - Human iPS cells derived cerebellar organoids
- METHOD DETAILS
  - Tamoxifen administration
  - Time-lapse video recording
  - Induction of Purkinje and granule cells from Sox2$^+$ cerebellar progenitors
  - Generation of MADM clones in cerebellum and tissue collection
  - Imaging and analysis of MADM-labeled brains
  - Cerebellar organoids staining
  - RNA extraction and real time PCR (RT-PCR)
  - Immunohistochemistry and antibodies
- QUANTIFICATION AND STATISTICAL ANALYSIS
  - Cell counts
  - scRNaseq quantification and statistical analyses
  - Statistical analysis

SUPPLEMENTAL INFORMATION

Supplemental information can be found online at https://doi.org/10.1016/j.celrep.2021.109208.

ACKNOWLEDGMENTS

This work was supported by the program "Investissements d'avenir" ANR-10-IAIHU-06, ICM, a Sorbonne Université Emergence grant, an Allen Distinguished Investigator Award, and the Roger De Spoelberch Foundation Prize (to B.A.H.); Armenise-Harvard Foundation, AIRC, and CARITRO (to L.T.); and the European Research Council under the European Union's Horizon 2020 research and innovation programme grant agreement no. 725780 LinPro (to S.H.). T.Z. and T.L. were supported by doctoral fellowships from the China Scholarship Council and A.H.H. by a doctoral DOC fellowship of the Austrian Academy of Sciences (24812). All animal work was conducted at the PHENO-ICMice facility. The Core is supported by 2 "Investissements d'avenir" (ANR-10- IAIHU-06 and ANR-11-INBS-0011-NeurATRIS) and the "Fondation pour la Recherche Médicale." Light microscopy work was carried out at ICM's imaging core facility, ICM.Quant, and analysis of scRNA-seq data was carried out at ICM's bioinformatics core facility, iCONICS. We thank Paulina Ejsmont, Natalia Danda, and Nathalie De Geest for technical support. We are grateful to Dr. Shahragim TAJBAKHSH for providing R26R$^{stop\text{-}NICD\text{-}nGFP}$ transgenic mice, Dr. Bart De Strooper for Psn1-deficient mice, Dr. Jean-Christophe Marine for *Gt(ROSA)26Sor*^{tdTom} reporter mice, and Dr. Martinez Barbera for *Sox2*^{CreERT2} mice. We also give thanks to Dr. Mikio Hoshino for providing Atoh1 and Ptf1a antibodies. B.A.H. is an Einstein Visiting Fellow of the Berlin Institute of Health.

AUTHOR CONTRIBUTIONS

B.A.H. and T.Z. designed the project and the experiments and prepared the manuscript with input from S.H. and L.T.; T.Z. and T.L. performed the majority of mouse experiments and data analysis; X.C., A.H.H., and C.S. performed the MADM experiments supervised by S.H.; N.D. helped with the preparation of MADM samples; M.A. performed the human organoid work supervised by

Figure 7. Notch GOF in ECPs inhibits their differentiation

(A) Immunostaining for Ptf1a$^+$ (red) in tdTomato$^+$ wild-type clones (gray) at E12. n = 4 embryos, totaling 51 clones in the VZ.
(B–B'') Higher magnification of the rectangular region in (A).
(C) Immunostaining for Ptf1a$^+$ (red) in NICD-GFP$^+$ clones (green) at E12. n = 4 embryos, totaling 11 clones in the VZ.
(D–D'') Higher magnification of the rectangular region in (C). Arrows indicate NICD-GFP$^+$/Ptf1a$^+$ double-positive cells.
(E) Percentage of Ptf1a$^+$ cells in control (tdTomato$^+$) versus NICD-GFP$^+$ VZ clones. ****$p < 0.0001$, t test.
(F) Immunostaining for Atoh1$^+$ (red) in tdTomato$^+$ wild-type clones (gray) at E12. n = 4 embryos, totaling 42 clones in the RL.
(G–G'') Higher magnification of the rectangular region in (F).
(H) Immunostaining for Atoh1$^+$ (red) in NICD-GFP$^+$ clones (green) at E12. n = 7 embryos, totaling 13 clones in the RL.
(I–I'') Higher magnification of the rectangular region in (H).
(J) Percentage of Atoh1$^+$ cells in control (tdTomato$^+$) versus NICD-GFP$^+$ RL clones. ****$p < 0.0001$, t test.
(K) Comparison of the ratios of Ptf1a$^+$ and Atoh1$^+$ cells in NICD-GFP$^+$ clones. **$p < 0.01$, t test.
(L) Immunostaining for Sox2$^+$ (red) in tdTomato$^+$ wild-type clones (gray) at E12. n = 4 embryos, totaling 28 clones in the RL and 30 clones in the VZ.
(M–M'') Higher magnification of the rectangular region in (L).
(N) Immunostaining for Sox2$^+$ (red) in NICD-GFP$^+$ clones at E12. n = 4 embryos, totaling 15 clones in the RL and 22 clones in the VZ.
(O–O'') Higher magnification of the rectangular region in (N).
(P) Percentage of Sox2$^+$ cells in control (tdTomato$^+$) versus NICD-GFP$^+$ RL and VZ clones. *$p < 0.05$; ****$p < 0.0001$, t tests.
Nuclei marked with DAPI (blue). Scale bars: 100 μm and 25 μm. Data are presented as mean ± SD.

L.T.; N.M. initiated the project; J.G. and M.B. performed bioinformatics analysis.

DECLARATION OF INTERESTS

The authors declare no competing interests.

INCLUSION AND DIVERSITY

We worked to ensure sex balance in the selection of non-human subjects.

Received: June 23, 2020
Revised: March 29, 2021
Accepted: May 11, 2021
Published: June 8, 2021

REFERENCES

Ahlfeld, J., Filser, S., Schmidt, F., Wefers, A.K., Merk, D.J., Glaß, R., Herms, J., and Schüller, U. (2017). Neurogenesis from Sox2 expressing cells in the adult cerebellar cortex. Sci. Rep. *7*, 6137.

Andreotti, J.P., Prazeres, P.H.D.M., Magno, L.A.V., Romano-Silva, M.A., Mintz, A., and Birbrair, A. (2018). Neurogenesis in the postnatal cerebellum after injury. Int. J. Dev. Neurosci. *67*, 33–36.

Apitz, H., and Salecker, I. (2018). Spatio-temporal relays control layer identity of direction-selective neuron subtypes in Drosophila. Nat. Commun. *9*, 2295.

Arnold, K., Sarkar, A., Yram, M.A., Polo, J.M., Bronson, R., Sengupta, S., Seandel, M., Geijsen, N., and Hochedlinger, K. (2011). Sox2(+) adult stem and progenitor cells are important for tissue regeneration and survival of mice. Cell Stem Cell *9*, 317–329.

Artavanis-Tsakonas, S., Rand, M.D., and Lake, R.J. (1999). Notch signaling: cell fate control and signal integration in development. Science *284*, 770–776.

Ballabio, C., Anderle, M., Gianesello, M., Lago, C., Miele, E., Cardano, M., Aiello, G., Piazza, S., Caron, D., Gianno, F., et al. (2020a). Modeling medulloblastoma in vivo and with human cerebellar organoids. Nat. Commun. *11*, 583.

Ballabio, C., Gianesello, M., Lago, C., Okonechnikov, K., Anderle, M., Aiello, G., Antonica, F., Zhang, T., Gianno, F., Giangaspero, F., et al. (2020b). Notch1 switches progenitor competence in inducing medulloblastoma. bioRxiv, 2020.05.10.084335.

Bauer, D.E., Jackson, J.G., Genda, E.N., Montoya, M.M., Yudkoff, M., and Robinson, M.B. (2012). The glutamate transporter, GLAST, participates in a macromolecular complex that supports glutamate metabolism. Neurochem. Int. *61*, 566–574.

Beattie, R., Postiglione, M.P., Burnett, L.E., Laukoter, S., Streicher, C., Pauler, F.M., Xiao, G., Klezovitch, O., Vasioukhin, V., Ghashghaei, T.H., and Hippenmeyer, S. (2017). Mosaic Analysis with Double Markers Reveals Distinct Sequential Functions of Lgl1 in Neural Stem Cells. Neuron *94*, 517–533.e3.

Bhat, K.M. (2014). Notch signaling acts before cell division to promote asymmetric cleavage and cell fate of neural precursor cells. Sci. Signal. *7*, ra101.

Bonnefont, J., Tiberi, L., van den Ameele, J., Potier, D., Gaber, Z.B., Lin, X., Bilheu, A., Herpoel, A., Velez Bravo, F.D., Guillemot, F., et al. (2019). Cortical Neurogenesis Requires Bcl6-Mediated Transcriptional Repression of Multiple Self-Renewal-Promoting Extrinsic Pathways. Neuron *103*, 1096–1108.e4.

Butler, A., Hoffman, P., Smibert, P., Papalexi, E., and Satija, R. (2018). Integrating single-cell transcriptomic data across different conditions, technologies, and species. Nat. Biotechnol. *36*, 411–420.

Carta, I., Chen, C.H., Schott, A.L., Dorizan, S., and Khodakhah, K. (2019). Cerebellar modulation of the reward circuitry and social behavior. Science *363*, eaav0581.

Carter, R.A., Bihannic, L., Rosencrance, C., Hadley, J.L., Tong, Y., Phoenix, T.N., Natarajan, S., Easton, J., Northcott, P.A., and Gawad, C. (2018). A Single-Cell Transcriptional Atlas of the Developing Murine Cerebellum. Curr. Biol. *28*, 2910–2920.e2.

Castro, D.S., Skowronska-Krawczyk, D., Armant, O., Donaldson, I.J., Parras, C., Hunt, C., Critchley, J.A., Nguyen, L., Gossler, A., Göttgens, B., et al. (2006). Proneural bHLH and Brn proteins coregulate a neurogenic program through cooperative binding to a conserved DNA motif. Dev. Cell *11*, 831–844.

Cleary, M.D., and Doe, C.Q. (2006). Regulation of neuroblast competence: multiple temporal identity factors specify distinct neuronal fates within a single early competence window. Genes Dev. *20*, 429–434.

Divya, T.S., Lalitha, S., Parvathy, S., Subashini, C., Sanalkumar, R., Dhanesh, S.B., Rasheed, V.A., Divya, M.S., Tole, S., and James, J. (2016). Regulation of Tlx3 by Pax6 is required for the restricted expression of Chrnα3 in Cerebellar Granule Neuron progenitors during development. Sci. Rep. *6*, 30337.

Doe, C.Q. (2017). Temporal Patterning in the *Drosophila* CNS. Annu. Rev. Cell Dev. Biol. *33*, 219–240.

Endo, K., Aoki, T., Yoda, Y., Kimura, K., and Hama, C. (2007). Notch signal organizes the Drosophila olfactory circuitry by diversifying the sensory neuronal lineages. Nat. Neurosci. *10*, 153–160.

Erclik, T., Li, X., Courgeon, M., Bertet, C., Chen, Z., Baumert, R., Ng, J., Koo, C., Arain, U., Behnia, R., et al. (2017). Integration of temporal and spatial patterning generates neural diversity. Nature *541*, 365–370.

Espinosa, J.S., and Luo, L. (2008). Timing neurogenesis and differentiation: insights from quantitative clonal analyses of cerebellar granule cells. J. Neurosci. *28*, 2301–2312.

Fink, A.J., Englund, C., Daza, R.A.M., Pham, D., Lau, C., Nivison, M., Kowalczyk, T., and Hevner, R.F. (2006). Development of the deep cerebellar nuclei: transcription factors and cell migration from the rhombic lip. J. Neurosci. *26*, 3066–3076.

Fleming, J.T., He, W., Hao, C., Ketova, T., Pan, F.C., Wright, C.C.V.V., Litingtung, Y., and Chiang, C. (2013). The Purkinje neuron acts as a central regulator of spatially and functionally distinct cerebellar precursors. Dev. Cell *27*, 278–292.

Gao, P., Postiglione, M.P., Krieger, T.G., Hernandez, L., Wang, C., Han, Z., Streicher, C., Papusheva, E., Insolera, R., Chugh, K., et al. (2014). Deterministic progenitor behavior and unitary production of neurons in the neocortex. Cell *159*, 775–788.

Goldowitz, D., Cushing, R.C., Laywell, E., D'Arcangelo, G., Sheldon, M., Sweet, H.O., Davisson, M., Steindler, D., and Curran, T. (1997). Cerebellar disorganization characteristic of reeler in scrambler mutant mice despite presence of reelin. J. Neurosci. *17*, 8767–8777.

Hachem, S., Laurenson, A.S., Hugnot, J.P., and Legraverend, C. (2007). Expression of S100B during embryonic development of the mouse cerebellum. BMC Dev. Biol. *7*, 17.

Hibi, M., and Shimizu, T. (2012). Development of the cerebellum and cerebellar neural circuits. Dev. Neurobiol. *72*, 282–301.

Hippenmeyer, S., Youn, Y.H., Moon, H.M., Miyamichi, K., Zong, H., Wynshaw-Boris, A., and Luo, L. (2010). Genetic mosaic dissection of Lis1 and Ndel1 in neuronal migration. Neuron *68*, 695–709.

Hori, K., Cholewa-Waclaw, J., Nakada, Y., Glasgow, S.M., Masui, T., Henke, R.M., Wildner, H., Martarelli, B., Beres, T.M., Epstein, J.A., et al. (2008). A nonclassical bHLH Rbpj transcription factor complex is required for specification of GABAergic neurons independent of Notch signaling. Genes Dev. *22*, 166–178.

Huang, X., Liu, J., Ketova, T., Fleming, J.T., Grover, V.K., Cooper, M.K., Litingtung, Y., and Chiang, C. (2010). Transventricular delivery of Sonic hedgehog is essential to cerebellar ventricular zone development. Proc. Natl. Acad. Sci. USA *107*, 8422–8427.

Imayoshi, I., Sakamoto, M., Yamaguchi, M., Mori, K., and Kageyama, R. (2010). Essential roles of Notch signaling in maintenance of neural stem cells in developing and adult brains. J. Neurosci. *30*, 3489–3498.

Ishida, Y., Kawakami, H., Kitajima, H., Nishiyama, A., Sasai, Y., Inoue, H., and Muguruma, K. (2016). Vulnerability of Purkinje Cells Generated from Spinocerebellar Ataxia Type 6 Patient-Derived iPSCs. Cell Rep. *17*, 1482–1490.

Ju, J., Liu, Q., Zhang, Y., Liu, Y., Jiang, M., Zhang, L., He, X., Peng, C., Zheng, T., Lu, Q.R., and Li, H. (2016). Olig2 regulates Purkinje cell generation in the early developing mouse cerebellum. Sci. Rep. *6*, 30711.

Kawasaki, H., Mizuseki, K., Nishikawa, S., Kaneko, S., Kuwana, Y., Nakanishi, S., Nishikawa, S.I., and Sasai, Y. (2000). Induction of midbrain dopaminergic neurons from ES cells by stromal cell-derived inducing activity. Neuron *28*, 31–40.

Kebschull, J.M., Ringach, N., Richman, E.B., Friedmann, D., Kolluru, S.S., Jones, R.C., Allen, W.E., Wang, Y., Zhou, H., Cho, S.W., et al. (2020). Cerebellar nuclei evolved by repeatedly duplicating a conserved cell type set. bioRxiv. https://doi.org/10.1101/2020.06.25.170118.

Kelberman, D., de Castro, S.C.P., Huang, S., Crolla, J.A., Palmer, R., Gregory, J.W., Taylor, D., Cavallo, L., Faienza, M.F., Fischetto, R., et al. (2008). SOX2 plays a critical role in the pituitary, forebrain, and eye during human embryonic development. J. Clin. Endocrinol. Metab. *93*, 1865–1873.

Kostadinov, D., Beau, M., Blanco-Pozo, M., and Häusser, M. (2019). Predictive and reactive reward signals conveyed by climbing fiber inputs to cerebellar Purkinje cells. Nat. Neurosci. *22*, 950–962.

Ladi, E., Nichols, J.T., Ge, W., Miyamoto, A., Yao, C., Yang, L.-T.T., Boulter, J., Sun, Y.E., Kintner, C., and Weinmaster, G. (2005). The divergent DSL ligand Dll3 does not activate Notch signaling but cell autonomously attenuates signaling induced by other DSL ligands. J. Cell Biol. *170*, 983–992.

Landry, C.F., Ivy, G.O., Dunn, R.J., Marks, A., and Brown, I.R. (1989). Expression of the gene encoding the β-subunit of S-100 protein in the developing rat brain analyzed by in situ hybridization. Brain Res. Mol. Brain Res. *6*, 251–262.

Laudet, V., Stehelin, D., and Clevers, H. (1993). Ancestry and diversity of the HMG box superfamily. Nucleic Acids Res. *21*, 2493–2501.

Leto, K., Arancillo, M., Becker, E.B.E., Buffo, A., Chiang, C., Ding, B., Dobyns, W.B., Dusart, I., Haldipur, P., Hatten, M.E., et al. (2016). Consensus Paper: Cerebellar Development. Cerebellum *15*, 789–828.

Li, P., Du, F., Yuelling, L.W., Lin, T., Muradimova, R.E., Tricarico, R., Wang, J., Enikolopov, G., Bellacosa, A., Wechsler-Reya, R.J., and Yang, Z.J. (2013a). A population of Nestin-expressing progenitors in the cerebellum exhibits increased tumorigenicity. Nat. Neurosci. *16*, 1737–1744.

Li, X., Erclik, T., Bertet, C., Chen, Z., Voutev, R., Venkatesh, S., Morante, J., Celik, A., and Desplan, C. (2013b). Temporal patterning of Drosophila medulla neuroblasts controls neural fates. Nature *498*, 456–462.

Machold, R.P., Kittell, D.J., and Fishell, G.J. (2007). Antagonism between Notch and bone morphogenetic protein receptor signaling regulates neurogenesis in the cerebellar rhombic lip. Neural Dev. *2*, 5.

Manto, M., Gandini, J., Feil, K., and Strupp, M. (2020). Cerebellar ataxias: an update. Curr. Opin. Neurol. *33*, 150–160.

Mayer, C., Hafemeister, C., Bandler, R.C., Machold, R., Batista Brito, R., Jaglin, X., Allaway, K., Butler, A., Fishell, G., and Satija, R. (2018). Developmental diversification of cortical inhibitory interneurons. Nature *555*, 457–462.

Mi, D., Li, Z., Lim, L., Li, M., Moissidis, M., Yang, Y., Gao, T., Hu, T.X., Pratt, T., Price, D.J., et al. (2018). Early emergence of cortical interneuron diversity in the mouse embryo. Science *360*, 81–85.

Miyazaki, T., Yamasaki, M., Hashimoto, K., Kohda, K., Yuzaki, M., Shimamoto, K., Tanaka, K., Kano, M., and Watanabe, M. (2017). Glutamate transporter GLAST controls synaptic wrapping by Bergmann glia and ensures proper wiring of Purkinje cells. Proc. Natl. Acad. Sci. USA *114*, 7438–7443.

Mora, N., Oliva, C., Fiers, M., Ejsmont, R., Soldano, A., Zhang, T.T., Yan, J., Claeys, A., De Geest, N., and Hassan, B.A. (2018). A Temporal Transcriptional Switch Governs Stem Cell Division, Neuronal Numbers, and Maintenance of Differentiation. Dev. Cell *45*, 53–66.e5.

Morales, D., and Hatten, M.E. (2006). Molecular markers of neuronal progenitors in the embryonic cerebellar anlage. J. Neurosci. *26*, 12226–12236.

Muguruma, K., Nishiyama, A., Kawakami, H., Hashimoto, K., and Sasai, Y. (2015). Self-organization of polarized cerebellar tissue in 3D culture of human pluripotent stem cells. Cell Rep. *10*, 537–550.

Murtaugh, L.C., Stanger, B.Z., Kwan, K.M., and Melton, D.A. (2003). Notch signaling controls multiple steps of pancreatic differentiation. Proc. Natl Acad. Sci. U S A *100*, 14920–14925.

Northcott, P.A., Robinson, G.W., Kratz, C.P., Mabbott, D.J., Pomeroy, S.L., Clifford, S.C., Rutkowski, S., Ellison, D.W., Malkin, D., Taylor, M.D., et al. (2019). Medulloblastoma. Nat. Rev. Dis. Primers *5*, 11.

Nowakowski, T.J., Bhaduri, A., Pollen, A.A., Alvarado, B., Mostajo-Radji, M.A., Di Lullo, E., Haeussler, M., Sandoval-Espinosa, C., Liu, S.J., Velmeshev, D., et al. (2017). Spatiotemporal gene expression trajectories reveal developmental hierarchies of the human cortex. Science *358*, 1318–1323.

Oberst, P., Fièvre, S., Baumann, N., Concetti, C., Bartolini, G., and Jabaudon, D. (2019). Temporal plasticity of apical progenitors in the developing mouse neocortex. Nature *573*, 370–374.

Peng, C.Y., Yajima, H., Burns, C.E., Zon, L.I., Sisodia, S.S., Pfaff, S.L., and Sharma, K. (2007). Notch and MAML signaling drives Scl-dependent interneuron diversity in the spinal cord. Neuron *53*, 813–827.

Pfeffer, C.K., and Beltramo, R. (2017). Correlating Anatomy and Function with Gene Expression in Individual Neurons by Combining *in Vivo* Labeling, Patch Clamp, and Single Cell RNA-seq. Front. Cell. Neurosci. *11*, 376.

Pibiri, V., Ravarino, A., Gerosa, C., Pintus, M.C., Fanos, V., and Faa, G. (2016). Stem/progenitor cells in the developing human cerebellum: an immunohistochemical study. Eur. J. Histochem. *60*, 2686.

Pinto-Teixeira, F., and Desplan, C. (2014). Notch activity in neural progenitors coordinates cytokinesis and asymmetric differentiation. Sci. Signal. *7*, pe26.

Qiu, X., Mao, Q., Tang, Y., Wang, L., Chawla, R., Pliner, H.A., and Trapnell, C. (2017). Reversed graph embedding resolves complex single-cell trajectories. Nat. Methods *14*, 979–982.

Quan, X.J., Yuan, L., Tiberi, L., Claeys, A., De Geest, N., Yan, J., van der Kant, R., Xie, W.R., Klisch, T.J., Shymkowitz, J., et al. (2016). Post-translational Control of the Temporal Dynamics of Transcription Factor Activity Regulates Neurogenesis. Cell *164*, 460–475.

Selvadurai, H.J., Luis, E., Desai, K., Lan, X., Vladoiu, M.C., Whitley, O., Galvin, C., Vanner, R.J., Lee, L., Whetstone, H., et al. (2020). Medulloblastoma Arises from the Persistence of a Rare and Transient Sox2^{+} Granule Neuron Precursor. Cell Rep. *31*, 107511.

Su, H.L., Muguruma, K., Matsuo-Takasaki, M., Kengaku, M., Watanabe, K., and Sasai, Y. (2006). Generation of cerebellar neuron precursors from embryonic stem cells. Dev. Biol. *290*, 287–296.

Telley, L., Govindan, S., Prados, J., Stevant, I., Nef, S., Dermitzakis, E., Dayer, A., and Jabaudon, D. (2016). Sequential transcriptional waves direct the differentiation of newborn neurons in the mouse neocortex. Science *351*, 1443–1446.

Vladoiu, M.C., El-Hamamy, I., Donovan, L.K., Farooq, H., Holgado, B.L., Sundaravadanam, Y., Ramaswamy, V., Hendrikse, L.D., Kumar, S., Mack, S.C., et al. (2019). Childhood cerebellar tumours mirror conserved fetal transcriptional programs. Nature *572*, 67–73.

Vong, K.I., Leung, C.K.Y., Behringer, R.R., and Kwan, K.M. (2015). Sox9 is critical for suppression of neurogenesis but not initiation of gliogenesis in the cerebellum. Mol. Brain *8*, 25.

Volpe, J.J., Inder, T.E., Darras, B.T., de Vries, L.S., du Plessis, A.J., Neil, J., and Perlman, J.M. (2017). Cerebellar development. Volpe's Neurology of the Newborn, Sixth Edition (Elsevier), pp. 73–99.

Wagner, M.J., and Luo, L. (2020). Neocortex-Cerebellum Circuits for Cognitive Processing. Trends Neurosci. *43*, 42–54.

Wang, V.Y., and Zoghbi, H.Y. (2001). Genetic regulation of cerebellar development. Nat. Rev. Neurosci. *2*, 484–491.

Wang, V.Y., Rose, M.F., and Zoghbi, H.Y. (2005). Math1 expression redefines the rhombic lip derivatives and reveals novel lineages within the brainstem and cerebellum. Neuron *48*, 31–43.

Wen, Y., Li, W., Choudhury, G.R., He, R., Yang, T., Liu, R., Jin, K., and Yang, S.H. (2013). Astroglial PTEN loss disrupts neuronal lamination by dysregulating radial glia-guided neuronal migration. Aging Dis. *4*, 113–126.

Wheeler, S.R., Stagg, S.B., and Crews, S.T. (2008). Multiple Notch signaling events control Drosophila CNS midline neurogenesis, gliogenesis and neuronal identity. Development *135*, 3071–3079.

Wojcinski, A., Lawton, A.K., Bayin, N.S., Lao, Z., Stephen, D.N., and Joyner, A.L. (2017). Cerebellar granule cell replenishment postinjury by adaptive reprogramming of Nestin^{+} progenitors. Nat. Neurosci. *20*, 1361–1370.

Yamada, K., Fukaya, M., Shibata, T., Kurihara, H., Tanaka, K., Inoue, Y., and Watanabe, M. (2000). Dynamic transformation of Bergmann glial fibers proceeds in correlation with dendritic outgrowth and synapse formation of cerebellar Purkinje cells. J. Comp. Neurol. *418*, 106–120.

Yamada, M., Seto, Y., Taya, S., Owa, T., Inoue, Y.U., Inoue, T., Kawaguchi, Y., Nabeshima, Y., and Hoshino, M. (2014). Specification of spatial identities of cerebellar neuron progenitors by ptf1a and atoh1 for proper production of GABAergic and glutamatergic neurons. J. Neurosci. *34*, 4786–4800.

Yang, Z.J., Ellis, T., Markant, S.L., Read, T.A., Kessler, J.D., Bourboulas, M., Schüller, U., Machold, R., Fishell, G., Rowitch, D.H., et al. (2008). Medulloblastoma can be initiated by deletion of Patched in lineage-restricted progenitors or stem cells. Cancer Cell *14*, 135–145.

Yusa, K., Zhou, L., Li, M.A., Bradley, A., and Craig, N.L. (2011). A hyperactive piggyBac transposase for mammalian applications. Proc. Natl. Acad. Sci. USA *108*, 1531–1536.

Zong, H., Espinosa, J.S., Su, H.H., Muzumdar, M.D., and Luo, L. (2005). Mosaic analysis with double markers in mice. Cell *121*, 479–492.

STAR★METHODS

KEY RESOURCES TABLE

REAGENT or RESOURCE	SOURCE	IDENTIFIER
Antibodies		
Rabbit anti-Sox2	Millipore	Cat# AB5603; RRID:AB_2286686
Rabbit anti-Sox2	abcam	ab97959; RRID:AB_2341193
Goat anti-Sox2	R&D Systems	Cat# AF2018; RRID:AB_355110
Rabbit anti-Calbindin	Immunostar	Cat# 24427; RRID:AB_10730728
Rabbit anti-Calbindin	Sigma	c2724-2; RRID:AB_258818
Rabbit anti-Pax6	Biolegend	Cat# PRB-278P; RRID:AB_291612
Mouse anti-Pax6	Synaptic Systems	Cat# 153011; RRID:AB_887758
Mouse anti-Pax6	SantaCruz	sc-53108; RRID:AB_630089
Rabbit anti-Pax2	Thermo	Cat#71-6000; RRID:AB_2533990
Mouse anti-Lhx1/5	DSHB	Cat# AB_531784; RRID:AB_531784
Goat anti-Olig2	R&D systems	Cat# AF2418; RRID:AB_2157554
Guinea pig anti-Tbr1	Synaptic Systems	Cat# 328 005; RRID:AB_2620072
Rabbit anti- GFP	Invitrogen	Cat# A-11122; RRID:AB_221569
Chicken anti-GFP	abcam	ab13970; RRID:AB_300798
Rabbit anti-Hes5	Sigma	AB5708; RRID:AB_91988
Rabbit anti-cleaved caspase 3	Cell Signaling	# 9661S; RRID:AB_2341188
Rabbit anti-Ptf1a	A kind gift from Dr. Mikio Hoshino	N/A
Rabbit anti-Atoh1	A kind gift from Dr. Mikio Hoshino	N/A
Goat anti-Rabbit IgG (H+L), Alexa Fluor™488	Invitrogen	A-11008; RRID:AB_143165
Donkey anti-Goat IgG (H+L), Alexa Fluor™488	Invitrogen	A-11055; RRID:AB_2534102
Goat anti-Guinea pig IgG (H+L), Alexa Fluor™488	Invitrogen	A-11073; RRID:AB_2534117
Goat anti-Chicken IgY (H+L), Alexa Fluor™488	Invitrogen	A-11039; RRID:AB_142924
Goat anti-Rabbit IgG (H+L), Alexa Fluor™555	Invitrogen	A-11034; RRID:AB_2576217
Goat anti-Mouse IgG (H+L), Alexa Fluor™555	Invitrogen	A-32727; RRID:AB_2633276
Donkey anti-Goat IgG (H+L), Alexa Fluor™555	Invitrogen	A-32816; RRID:AB_2762839
Goat anti-Rabbit IgG (H+L), Alexa Fluor™647	Invitrogen	A-21245; RRID:AB_2535813
Goat anti-Mouse IgG (H+L), Alexa Fluor™647	Invitrogen	A-21235; RRID:AB_2535804
Chemicals, peptides, and recombinant proteins		
DAPI	Sigma	Cat# D9564
DAPI	Invitrogen	Cat#62248
Tamoxifen	Sigma	Cat#T5648
(Z)-4-Hydroxytamoxifen	Sigma	Cat#H7904
Corn oil	Sigma	Cat#C8267
Triton X-100	Sigma	Cat#X100
Trizol Reagent	Invitrogen	Cat#15596026
QuantiTect Reverse Transcription Kit	QIAGEN	Cat# 205311
LightCycler® 480 SYBR Green I Master	Roche	Cat# 04707516001
Tissue-Tek O.C.T	Sakura	Cat# 4583
Frozen Section Compound	Leica	3801480
Mounting Medium	Vector Laboratories	Cat#H-1000
Geltrex	GIBCO	Cat# A14133-01
E8 Basal Medium	GIBCO	Cat# A15169-01
EDTA	Invitrogen	Cat# 15575-038

(*Continued on next page*)

CellPress
OPEN ACCESS

Continued

REAGENT or RESOURCE	SOURCE	IDENTIFIER
DBZ	Sigma	Cat# SML0649
poly-L-ornithine hydrobromide	Sigma	P4957
laminin	Sigma	L2020
L15 medium	GIBCO	11415064
0.05% trypsin/EDTA	GIBCO	25300-054
SVF	Invitrogen	10270106
DNase	Serlabo	LS002138
Neurobasal medium without phenol red	GIBCO	12348-017
B27 supplement	GIBCO	17504-044
L-glutamax	GIBCO	35050-061
Mouse epidermal growth factor	Thermofisher	PMG8041
Mouse basic fibroblast growth factor	Thermofisher	PMG0035
HEPES	GIBCO	12509079
insulin	Sigma	I0516
α-MEM medium	GIBCO	12561056
KSR	GIBCO	10828010
2-ME	GIBCO	31350010
BMP4	R&D	5020-BP-010
Neurobasal-Plus	GIBCO	A3582901
B27-Plus	GIBCO	A3582801
Ascorbic acid	Sigma	A4403
Superfrost Ultra Plus Adhesive Blades	Thermofisher	Thermofisher
Deposited data		
single-cell RNA sequencing (scRNaseq) data	Carter et al., 2018	ENA: PRJEB23051 dataset
Experimental models: Cell lines		
Human iPS cells	ATCC	Cat# DYS0100; RRID:CVCL_X499
Experimental models: Organisms/strains		
Sox2^{CreERT2}	The Jackson Laboratory	JAX stock #017593; RRID:IMSR_JAX:017593
Gt(ROSA)26Sor^{tdTom}	The Jackson Laboratory	JAX stock #007914; RRID:IMSR_JAX:007914
R26R$^{stop\text{-}NICD\text{-}nGFP}$	The Jackson Laboratory	JAX stock #008159; RRID:IMSR_JAX:008159
Presenilin1 (*Psn*$^{-/-}$)	A gift from Bart De Strooper's lab	N/A
Atoh1^{GFP}	A gift from Huda Zoghbi's Lab	N/A
Notch1^{flox}	The Jackson Laboratory	JAX stock #007181; RRID:IMSR_JAX:007181
MADM-11^{TG}	The Jackson Laboratory	JAX stock #013751; RRID:IMSR_JAX:013751
MADM-11^{GT}	The Jackson Laboratory	JAX stock #013749; RRID:IMSR_JAX:013749
Oligonucleotides		
PCR primers for genotyping	IDT	See Table S3
PT-PCR primers	IDT	See Table S3
Recombinant DNA		
pCAG PiggyBac (PBase)	Yusa et al., 2011	A gift from https://www.sanger.ac.uk/
piggyBac donor plasmid pPB CAG Venus	Ballabio et al., 2020a	A gift from https://www.sanger.ac.uk/form/Sanger_CloneRequests
pGL3-Sox2	Addgene Plasmid	#101761; RRID:Addgene_101761
pGL3-Sox2Cre	This manuscript	N/A
pPB CAG LSL Venus	This manuscript	N/A
Software and algorithms		
Prism 7.0	GraphPad Software	https://www.graphpad.com/
ImageJ	ImageJ	https://imagej.nih.gov/ij/download.html

(*Continued on next page*)

Continued

REAGENT or RESOURCE	SOURCE	IDENTIFIER
Umitools	GitHub	https://github.com/weng-lab/umitools
Seurat bioconductor package v2.3.4	Satija Lab	https://satijalab.org/seurat/
Monocle 2.6.4	GitHub	https://github.com/cole-trapnell-lab/monocle-release
Allen Brain Atlas	Allen Brain Atlas	http://mouse.brain-map.org/static/atlas
Photoshop software	Adobe	https://www.adobe.com/
Zeiss Zen Blue software	Zeiss	https://www.zeiss.com/corporate/int/home.html
FV-OSR software	Olympus	https://www.olympus-lifescience.com/en/
LAS X Core software	Leica	https://www.leica-microsystems.com/
Other		
Confocal microscope	Olympus	FV-1200
Confocal microscope	Leica	SP8X
Confocal microscope	Zeiss	LSM800
Rotary cryostat microtome	Leica	CM3050 S
Videomicroscope	Zeiss	AxioObserver 7

RESOURCE AVAILABILITY

Lead contact

Further information and requests for resources and reagents should be directed to and will be fulfilled by the lead contact, Bassem Hassan (bassem.hassan@icm-institute.org).

Materials availability

This study did not generate new unique reagents.

Data and code availability

This study did not generate any unique datasets. All RNA-seq data in this study were retrieved from ENA: PRJEB23051 dataset.

EXPERIMENTAL MODEL AND SUBJECT DETAILS

Mice

All animal experiments in this study were carried out in accordance with animal welfare regulations and have been approved by Ethic Committee and French regulatory authorities of the respective institutes. The *Sox2*^{CreERT2} mice were crossed with *Gt(ROSA) 26Sor*^{tdTom} reporter mice, and then crossed with *Atoh1*^{GFP} mice to generate the lineage tracing line. Notch gain-of-function mice were generated by breeding *Sox2*^{CreERT2}/ *Gt(ROSA)26Sor*^{tdTom} with *R26R*$^{stop\text{-}NICD\text{-}Ngfp}$ (Murtaugh et al., 2003). Presenilin1 deficient (*Psn*$^{-/-}$) mice crossed with *Atoh1*^{GFP} mice to get *Atoh1*^{GFP}/*Psn*$^{-/-}$ mice. And Notch conditional knock out mice was generated by crossing *Notch1*^{flox} with *Sox2*^{CreERT2}/ *Atoh1*^{GFP} mice. Mice were genotyped genomic DNA isolated from toe tissue. Primers used for genotyping can be found in Table S3.

Primary culture of mouse cerebellar progenitor cells

Preparation

Two days before cell isolation, 13mm coverslips were placed in a 24 well plate, then the plate was coated with 500 ul poly-L-ornithine hydrobromide (Sigma, P4957) and incubated overnight. Next, the plate was washed 3 times with sterile water, then coated with 500 ul laminin (Final conc: 5ug/ml, Sigma, L2020) and incubated overnight.

Isolation and culture of cerebellar progenitor cells

Cerebellar progenitors were harvested from *Sox2*^{CreERT2}/ *Gt(ROSA)26Sor*^{tdTomtato} pregnant mice. In brief, cerebella were dissected from E11.5 mouse embryos in L15 medium (GIBCO, 11415064) and enzymatically dissociated to single cells using 0.05% trypsin/ EDTA (GIBCO, 25300-054) plus 30% SVF (Invitrogen, 10270106) plus DNase (Serlabo, LS002138). The cells were collected and re-suspended in proliferation medium: Neurobasal medium without phenol red (GIBCO, 12348-017) containing B27 supplement (GIBCO, 17504-044), L-glutamax (GIBCO, 35050-061), 20 ng/ml mouse epidermal growth factor (EGF, Thermofisher, PMG8041), 10 ng/ml mouse basic fibroblast growth factor (bFGF, Thermofisher, PMG0035), 1M HEPES (GIBCO, 12509079) and insulin (Sigma, I0516). Cells were plated on coverslips in a precoated 24-well plate with 0.05 ng/ml Tamoxifen treatment, then cultured at 37°C with 5% CO_2 in an incubator (Thermo Scientific).

MADM mouse lines and maintenance

MADM employs Cre recombinase/loxP-dependent interchromosomal recombination highlighting two scenarios: (i) Recombination occurs in G2 phase of the cell cycle with X segregation (G2-X MADM clone) can create two distinctly labeled daughter cell lineages from their common mother progenitor cell; (ii) Recombination occurs in G1 phase or in G2 phase followed by Z segregation (G1/G2-Z MADM clone), one or both daughter cell lineages will be labeled in yellow. Mouse protocols were reviewed by institutional ethics committee and preclinical core facility (PCF) at IST Austria and all breeding and experimentation was performed under a license approved by the Austrian Federal Ministry of Science and Research in accordance with the Austrian and EU animal laws (license numbers: BMWF-66.018/0007-II/3b/2012 and BMWFW-66.018/0006-WF/V/3b/2017).. Mice were maintained and housed in animal facilities with a 12-hour day/night cycle and adequate food/water conditions according to IST Austria institutional regulations. Mouse lines with Chr. 11 MADM cassettes (MADM-11^{TG} and MADM-11^{GT}), and *Sox2-CreER* have been described previously (Arnold et al., 2011; Hippenmeyer et al., 2010). All MADM-based analyses were carried out in a mixed C57BL/6J, CD1 genetic background.

Human iPS cells derived cerebellar organoids

Cerebellar organoids generation and labeling

Cerebellar organoids were culture as described by Muguruma et al. (2015) and Ishida et al. (2016). Human iPS cells (iPSCs, ATCC-DYS0100) were maintained in self-renewal on a layer of geltrex (GIBCO, A14133-01), in E8 Basal Medium (GIBCO, A15169-01) supplemented with E8 Supplement (50X). iPSC were dissociated with EDTA (Invitrogen) 0.5mM, pH 8.0, for 3 minutes incubation, to maintain cell clusters. 6000 cell/well were seed in 96 well (Sumitomo Bakelite) in differentiation medium (see Muguruma et al., 2015). One-third dilution and a full-volume replacement with medium were performed on day 7 and 14, respectively. On day 2, the aggregates were transferred from the 96 to 6 well non-tissue treated, to cultured in Neurobasal medium with Glutamax and N2 supplement. In order to sparsely label potential Sox2^{+} human ECPs, organoids were electroporated at 25d with 20ug pCAG PiggyBac (PBase), 80 ug pPB CAG LSL Venus and 20ug pGL3-SOX2Cre (for DBZ experiment); with 80 ug pPB CAG LSL Venus and 20ug pGL3-SOX2Cre (for cell 24h experiment). Organoids were transferred inside the Electroporation cuvettes (VWR, ECN 732-1136, 2mm) resuspended in Buffer 5 (under patent) and electroporation was performed with the Gene Pulser XcellTM.

The plasmid encoding an hyperactive form of the piggyBac transposase (pCMV HAhyPBase, pPBase) was a gift from https://www.sanger.ac.uk/ (Yusa et al., 2011). The piggyBac donor plasmid pPB CAG Venus were previously described (Ballabio et al., 2020a). The pSox2-cre plasmid was generated by cloning the cre coding sequence into pGL3-Sox2 (Addgene Plasmid #101761). The plasmid was used as backbone to insert before the start codon a loxP-STOP-loxP cassette by PCR, generating pPB CAG LSL Venus.

DBZ experiment: organoids were treated from days 27 to 31 of differentiation, with 1 dose of 10 μM DBZ (Notch inhibitor) or DMSO, and then changed the medium at 31 d.

METHOD DETAILS

Tamoxifen administration

Tamoxifen (TM, Sigma) or 4-Hydroxytamoxifen (4-OH, Sigma) was dissolved to a final concentration of 1mg/ml or 3mg/ml in 90% corn oil (Sigma) with 10% ethonal (Sigma). For lineage tracing experiments (*Sox2^{CreERT2}/ Gt(ROSA)26Sor^{tdTom} / Atoh1^{GFP}* mice), if collected the samples at embryonic stages (E11, E14, E15 and E16), 0.03mg or 0.1mg TM was intraperitoneal (i.p.) injected into per pregnant female at E9.5, E10.5 or E13.5. If collected the samples at postnatal stages (P21), each pregnant female was injected 0.03mg or 0.05mg TM (i.p.) at E10.5 or E11.5. For Notch loss of function experiments (*Sox2^{CreERT2}/ Atoh1^{GFP}/ Notch1^{flox}* mice), 0.3mg TM was injected into the pregnant females (i.p.) at E8.5, and samples were collected at E12. For Notch gain of function experiments (*Sox2^{CreERT2}/Gt(ROSA)26Sor^{tdTom}/R26R$^{stop\text{-}NICD\text{-}nGFP}$* mice), 0.3mg 4-OH TM was injected into the pregnant females (i.p.) at E8.5, and samples were collected both at E12 and E16.

Time-lapse video recording

Primary cultured progenitor cell proliferation was tracked using time-lapse video recording. Two hours after cell seeding, the 24-well plate was transferred to a videomicroscope (Zeiss AxioObserver 7) with a humidified incubator at 37°C with a constant 5% CO_2 supply. Timlapse images for both Cy3 and bright field were acquired every 30 min, 45 min and 60 min for for 72 hours, day 4 and day 5 and day 6-day12, respectively (Videos S1 and S2, related to Figure 3).

Induction of Purkinje and granule cells from Sox2^{+} cerebellar progenitors

Three days after time-Lapse Video Recording, the proliferation medium was changed to differentiation medium as described previously (Kawasaki et al., 2000; Su et al., 2006). First, to induce Pax6^{+} granule neurons, cells were cultured in α-MEM medium (GIBCO, 12561056) supplemented with 5% KSR (GIBCO, 10828010), 0.1mM 2-ME (GIBCO, 31350010) and 0.5 nM mouse BMP4 (R&D, 5020-BP-010). Three days later, the medium was changed to Neurobasal-Plus (GIBCO, A3582901) supplemented with B27-Plus (GIBCO, A3582801), Ascorbic acid (Sigma, A4403) and 0.5 nM mouse BMP4 in order to induce the production of Calbindin^{+} Purkinje neurons. At the end of the 12 days of recording, cells were fixed directly by using 4% PFA and immunostaining was performed.

Generation of MADM clones in cerebellum and tissue collection

To induce MADM labeling, *MADM-11*$^{GT/GT}$/*Sox2*^{CreER} were crossed with *MADM-11*$^{TG/TG}$ in order to generate experimental mice *MADM-11*$^{GT/TG}$/*Sox2*^{CreER}. The day of observed vaginal plug was defined as E0 to monitor gestation days. Pregnant mice were injected i.p. with TM (2-3 mg/pregnant female) (Sigma, T5648) dissolved in corn oil (Sigma, C8267) at E10 or E11 to induce MADM clones. Live embryos were recovered at E18–E19 through cesarean section, fostered, and raised until further analysis. At P21 experimental MADM mice were deeply anesthetized through injection of a ketamine/xylazine/acepromazine solution (65 mg, 13 mg and 2 mg/kg body weight, respectively), and confirmed to be unresponsive through pinching the paw. Mice were perfused transcardially with 4% PFA in phosphate-buffered saline (PBS, pH 7.4). Brains were removed and postfixed o/n at 4°C to ensure complete fixation. Brains were washed with PBS, and cryopreserved with 30% sucrose solution in PBS for approximately 48 hr. Brains were then embedded in Tissue-Tek O.C.T. (Sakura, #4583). For the analysis of MADM labeling, 35μm sagittal sections were directly and consecutively collected throughout the entire cerebellum and fixed to superfrost glass slides (Thermo Fisher Scientific, J3800AMNT). Sections were washed 3 times for 5 min with PBS, followed by staining with the nuclear stain DAPI (Invitrogen, 62248). After this step the slides were again washed 3 times with PBS and embedded in mounting medium(Vector Laboratories, Cat#H-1000). .

Imaging and analysis of MADM-labeled brains

Sections were imaged using confocal microscopes (Zeiss-LSM800, Olympus FV-1200 or Leica SP8X)) and processed using Zeiss Zen Blue, FV-OSR or LAS X Core softwares. Confocal images were analyzed in Photoshop software (Adobe) and ImageJ by manually counting MADM-labeled cells. Cerebellar areas were identified by using the Allen Brain Atlas (http://mouse.brain-map.org/static/atlas).

Cerebellar organoids staining

Organoids were fixed at 26d or 41d of differentiation with 4% PFA, cryoprotected in 20% sucrose and embedded in Frozen Section Compound (Leica, 3801480). Organoids were cryosectioned at 40 μm with Leica CM 1850 UV Cryostat. Immunofluorescence staining were performed on glass slides. Blocking and antibody solutions consisted of PBS supplemented with 3% goat serum, 0.3% Triton X-100 (Sigma, X100). Primary antibodies were incubated overnight at 4°C and secondary antibodies for 1 hour at RT. Primary antibodies used were Chicken anti-GFP (1:2000, abcam, ab13970), Rabbit anti-Sox2 (1:500, abcam, ab97959), Mouse anti-Pax6 (1:100, SantaCruz, sc-53108)and Rabbit anti-Calbindin (1:500, Sigma, c2724-2). Nuclei were stained with 1 μg/ml DAPI (Sigma). Sections and coverslips were mounted with Permanent Mounting Medium.

RNA extraction and real time PCR (RT-PCR)

Total RNA was isolated from whole cerebellar tissue samples at E13 using Trizol Reagent (Invitrogen, 15596026). The RNA concentration was measured by a spectrophotometer (NanDrop1000; Thermo) followed by a reverse transcription process using QuantiTect Reverse Transcriptase kit (QIAGEN, 205311). Real time PCR analysis was performed using SYBR green mix (Roche, 04707516001). PCR conditions used here were denaturing at 95°C for 10 s, followed by 40 cycles of 95°C for 5 s and 60°C for 30 s. Data were analyzed using the comparative threshold cycle (Ct) method, and results were expressed as fold difference normalized to GAPDH.Primers used for RT-PCR can be found in Table S3.

Immunohistochemistry and antibodies

For the samples collection, embryos before E13.5 were fixed in 2% paraformaldehyde (PFA) in PBS at 4°C for 2-3 hours, and embryos after E13.5 but before born first were perfused with 2% PFA, then post-fixed for 24 hours. Whereas, samples were collected at postnatal stages, perfused the mice with 1 X PBS, followed by 4% PFA perfusion, and then post-fixed in 4% PFA for another 24 hours. Dehydrated embryos or the whole head in 30% sucrose in 1 X PBS overnight (o/n). After all the samples sank into the bottom of the tube, embedded them in OCT compound (TissueTek, # 4583) and frozen at −20°C. Sagittal sections were made by cryostat (Leica, CM3050 S) at 20 μm and then stored slices at −80°C. For the immunostaining, sections were fixed with 4% PFA for 10 minutes at room temperature (RT), then blocked with 10% normal donkey or goat serum in 1 X PBS with 0.1% Triton (PBT) for 1 hour at RT followed by 3 times washing in 1 XPBT. Thereafter, these sections were incubated with primary antibodies diluted in 0.1% 1 X PBT containing 1% normal donkey or goat serum o/n at 4°C or 3-4 hours at RT. After 3 times washing with 1 X PBT, incubated with appropriate secondary antibodies conjugated with Alexa Fluor 488, Alexa Fluor 555, or Alexa Fluor 647 (1:500, Invitrogen) in 0.1% 1 X PBT containing 1% normal donkey or goat serum for 1-2 hours at RT. Washed with 1 X PBT for 3 times, then counterstained the slides with DAPI (1:2000, Sigma, D9564) and mounted by using Vectashield (Vector, H-1000) after rinsing. Antigen retrieval was performed by using 10 mM sodium citrate buffer, pH 6.0, boiled 5 minutes in microwave, and cooled down in RT for about 20 minutes for Lhx1/5 and Olig2 staining. Primary antibodies used in this study were rabbit anti-Sox2 (1:500, Millipore, AB5603), rabbit anti-Ptf1a and Rabbit anti-Atoh1 (1:200, a kind gift from Dr. Mikio Hoshino, National Center of Neurology and Psychiatry · Department of Biochemistry and Cellular Biology, Japan), rabbit anti-Calbindin (1:500, Immunostar, 24427), rabbit anti-Pax6 (1:300, Biolegend: PRB-278P), mouse anti-Pax6 (1:300, Synaptic Systems: 153011), rabbit anti-Pax2 (1:200, Thermo, QE215176), mouse anti-Lhx1/5 (1:100, DSHB, AB_531784), goat anti-Olig2 (1:500, R&D systems, AF2418), Guinea pig anti-Tbr1 (1:500, Synaptic Systems, 328 005), Rabbit

anti-Hes5 (1:200, Sigma, AB5708) and Rabbit anti- Cleaved Caspase-3 (1:200, cell signaling, 9661S). After staining, images were obtained by using confocal microscope (Olympus FV-1200 or Leica SP8X).

QUANTIFICATION AND STATISTICAL ANALYSIS

Cell counts

For the Notch loss of function and Notch gain of function parts, confocal images for single layer scanning of sagittal cerebellar sections were calculated for each developmental stage (E12 and E13) after DAPI staining by using ImageJ (https://imagej.nih.gov/ij/download.html). Each section took the sum of the four values that obtained from 4 single layer calculating, which could form a Z stack. And each cerebellar sample counted 6-8 sections that took from the beginning to the end of the cerebellum. All quantifications were done blinded to the genotyping. For each stage littermates were analyzed and all groups of quantifications were carried out from at least 3 individuals. For the specific number of embryos, please see the figure legends.

scRNaseq quantification and statistical analyses

Aligned 10X data were retrieved from ENA: PRJEB23051 dataset for the following samples: E10, E11, E12 and E13. Umitools has been used to generate gene-cell matrices with the following parameters:–extract-umi-method = tag,–umi-tag UB,–cell-tag CB,–per-gene,–gene-tag GX,–per-cell. Genes not expressed in any cells were removed from considerations, as were all mitochondrial and ribosomal protein genes. To remove likely dead or multiplet cells from downstream analyses, cells were discarded if they had less than 3500 UMIs, greater than 15000 UMIs, or were composed of over 10% mitochondrial UMIs. The final dataset was composed of 14637 cells and 18937 genes. Then Seurat bioconductor package v2.3.4 (Butler et al., 2018) has been used to do cell-cell comparison and identify cell types. First, we performed a t-SNE (t-distributed stochastic neighbor embedding) with the first 20 principal components after application of PCA reduction. This allowed us to visualize the grouping of cells and the expression of genes of interest. Expression of cells in 3 populations has been represented with violin plot and differential expression between the 3 populations has been calculated with a Welch two sample t test procedure.

Monocle 2.6.4 (Qiu et al., 2017) was used to infer the pseudotime trajectory. As we worked with UMI count data, we assumed that the data were distribued among a negative binomial distribution with fixed variance. The genes that ‘‘define progress’’ were selected using the unserpervised procedure ‘‘dpFeature’’: we first selected genes expressed in at least 5% of all the cells. We then run reduceDimension with tSNE as the reduction method, num_dim = 10,’’ norm_method = ’’log’’ and max_components = 2. Finally, cells were clustered with the density peak clustering algorithm by setting P to 2 and Δ to 5 (and skip_rho_sigma = T to facilitate the computation). The top 1000 significantly differentially expressed genes between clusters were selected as the ordering genes. The state 3 where Sox2 is expressed and Atoh1 not expressed was defined as the start of the pseudotime. The seurat FindMarkers function was used to identify the top 10 genetic markers of each lineage state’s.

Statistical analysis

Statistical analyses were performed using GraphPad Prism software (GraphPad Software Inc., La Jolla, CA, USA). N values refers to independent animals and are detailed in the figure legends. All data are presented as mean ± SEM. Statistical testing was based on t tests or one-way ANOVA, followed by Tukey’s honest significant test. Details on the statistical tests used for each experiment are located in the figure legends.

Cell Reports, Volume *35*

Supplemental information

Generation of excitatory and inhibitory neurons from common progenitors via Notch signaling in the cerebellum

Tingting Zhang, Tengyuan Liu, Natalia Mora, Justine Guegan, Mathilde Bertrand, Ximena Contreras, Andi H. Hansen, Carmen Streicher, Marica Anderle, Natasha Danda, Luca Tiberi, Simon Hippenmeyer, and Bassem A. Hassan

Figure S1: Sox2 is highly expressed both in the RL and VZ

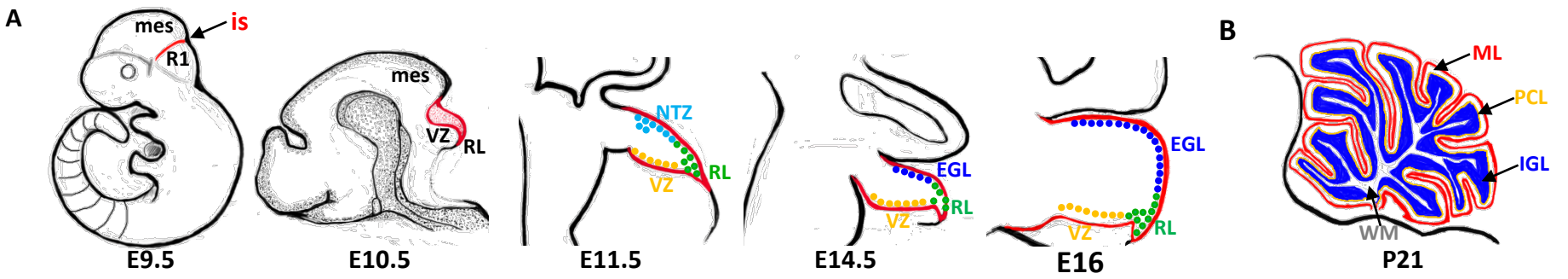

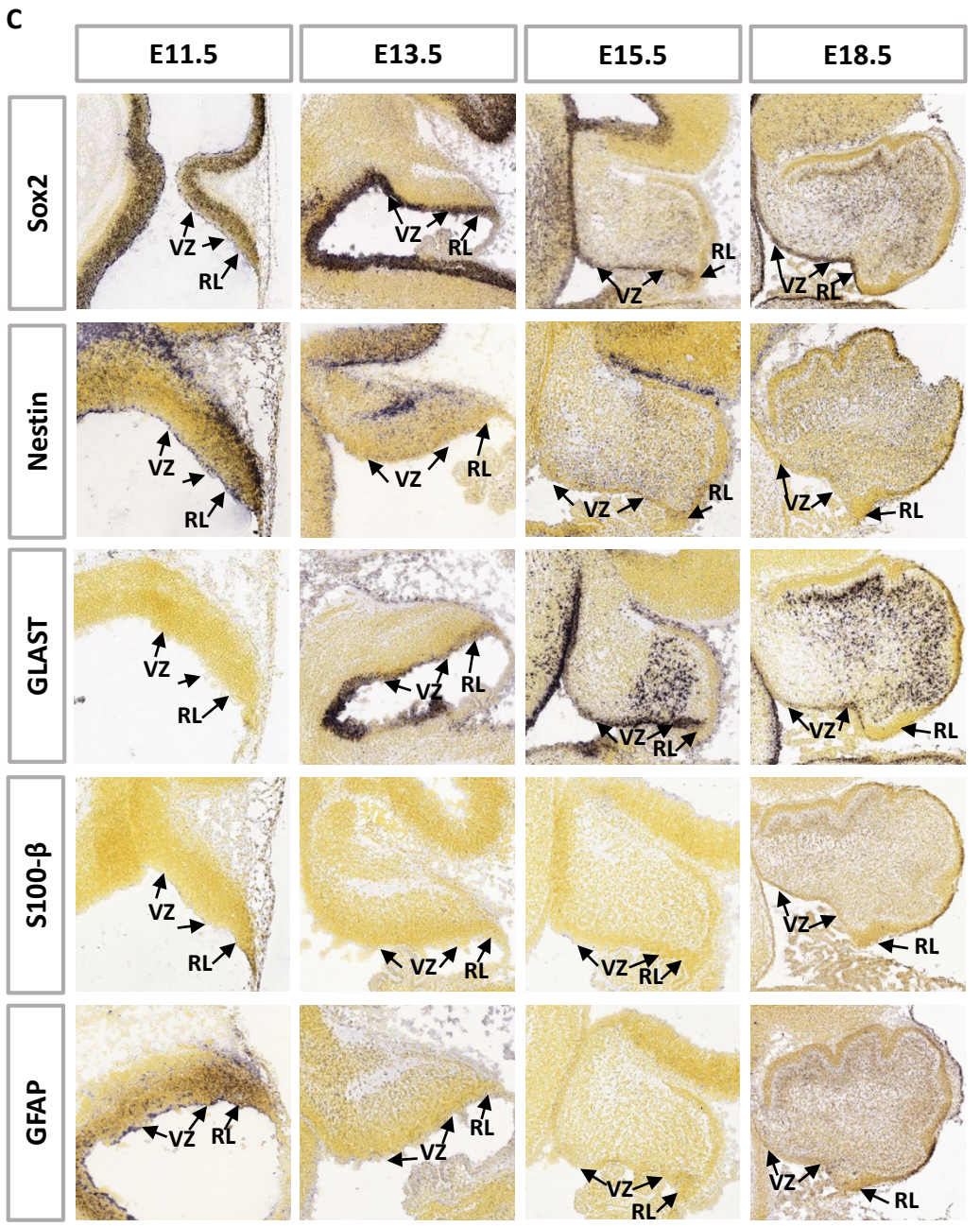

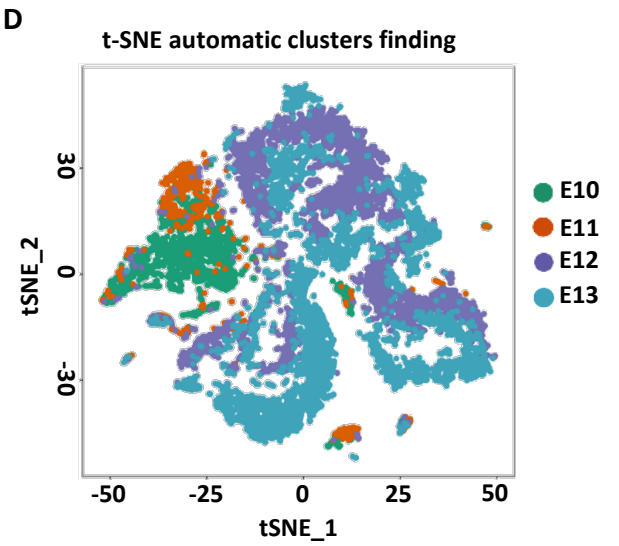

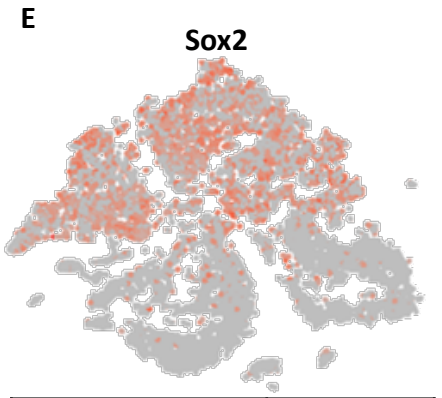

	Number
Sox2⁺/Nestin⁻	1313
Sox2⁺/Nestin⁺	1314

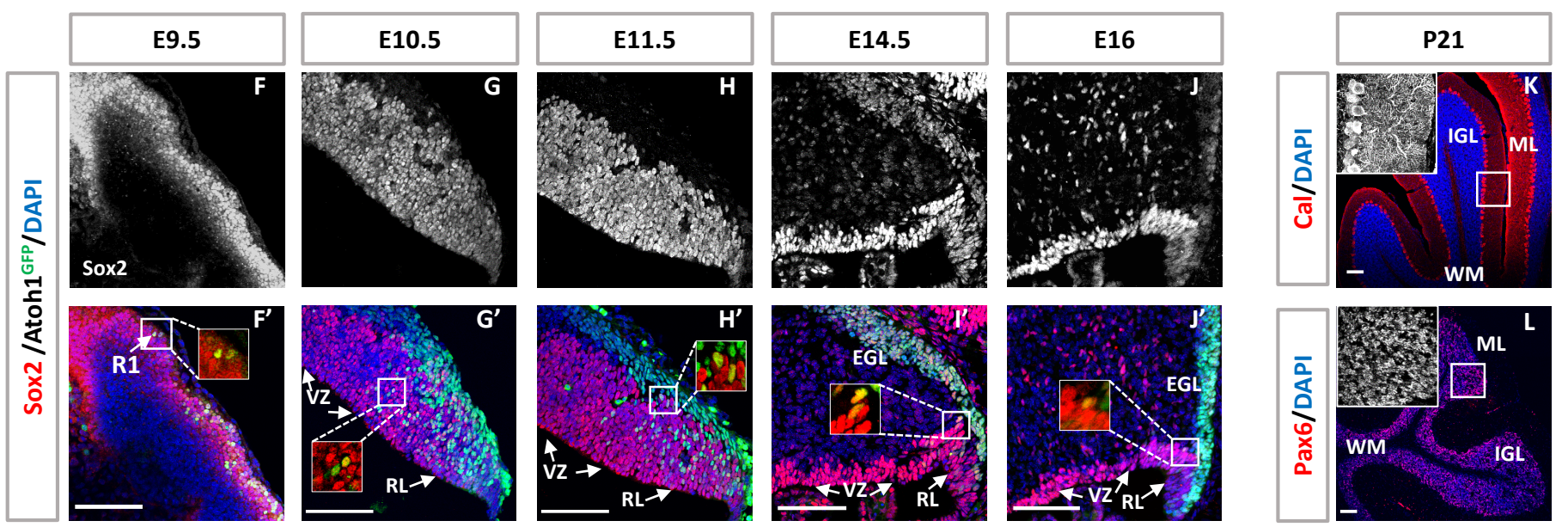

Figure S2: Sox2 progenitors give rise to the different cerebellar neuronal subtypes

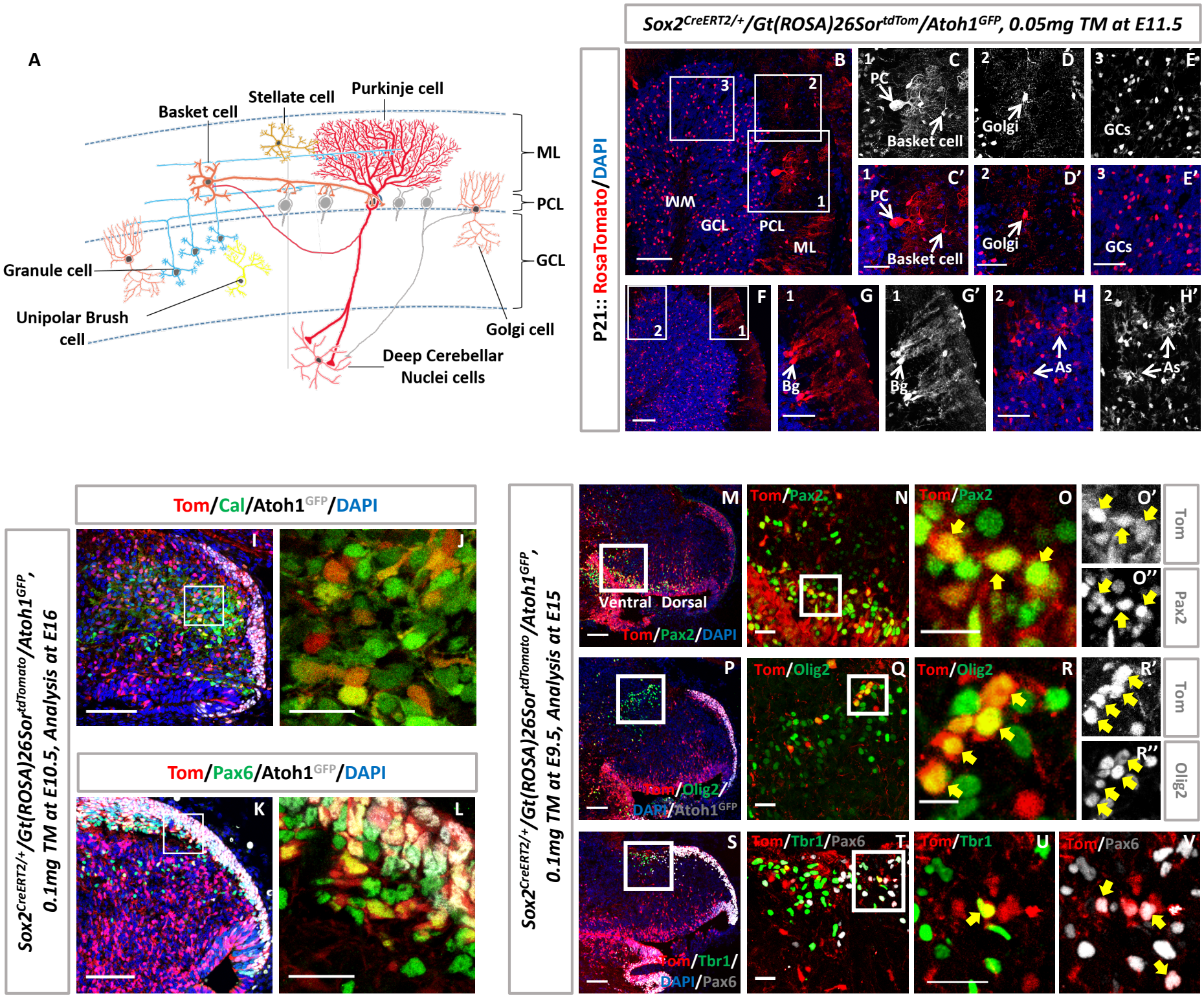

Figure S3: Sparse lineage tracing of ECPs both in the mouse cerebellum and in human cerebellar organoids

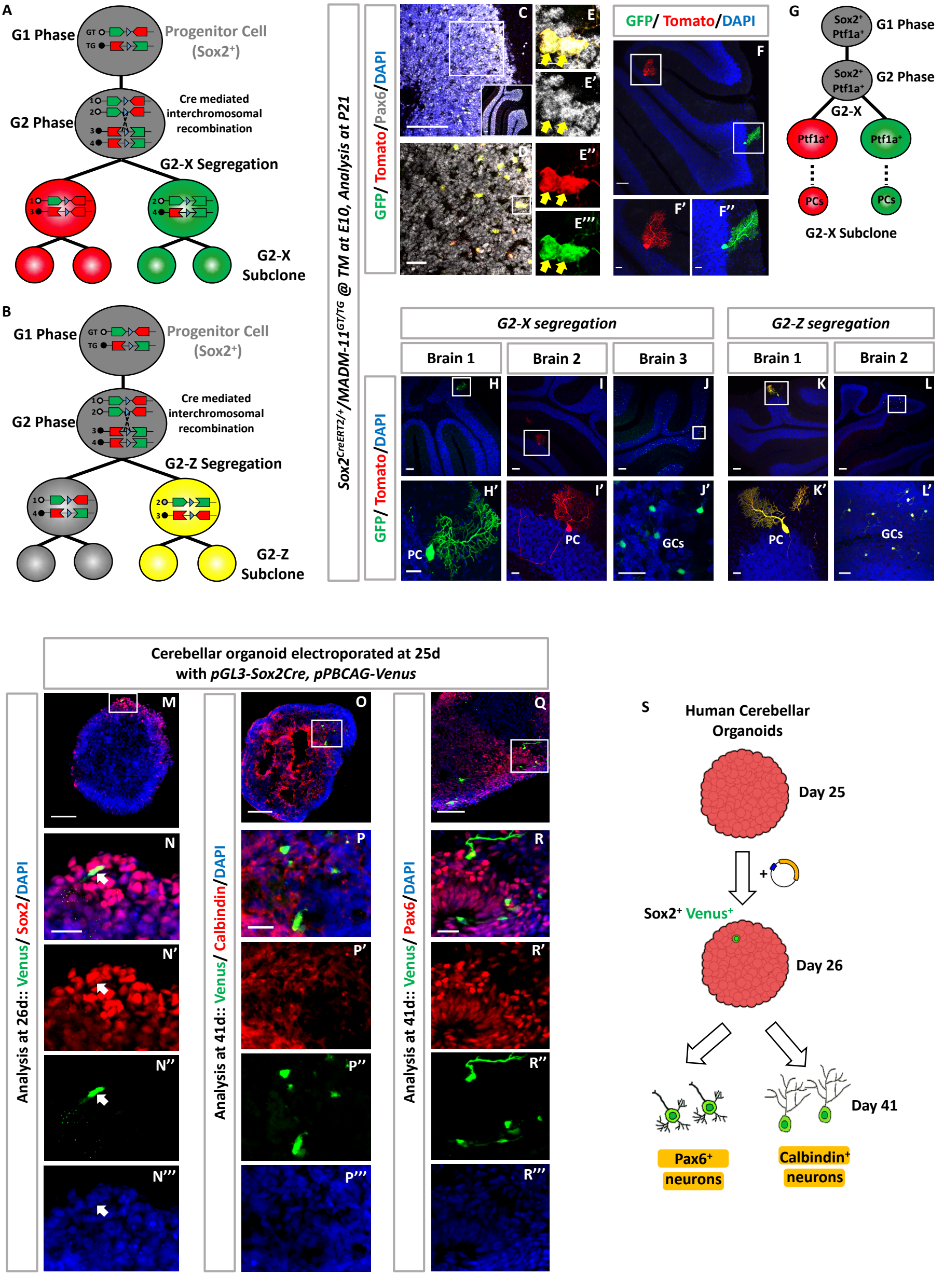

Figure S4: Notch loss of function increases RL progenitors at the expense of VZ progenitors

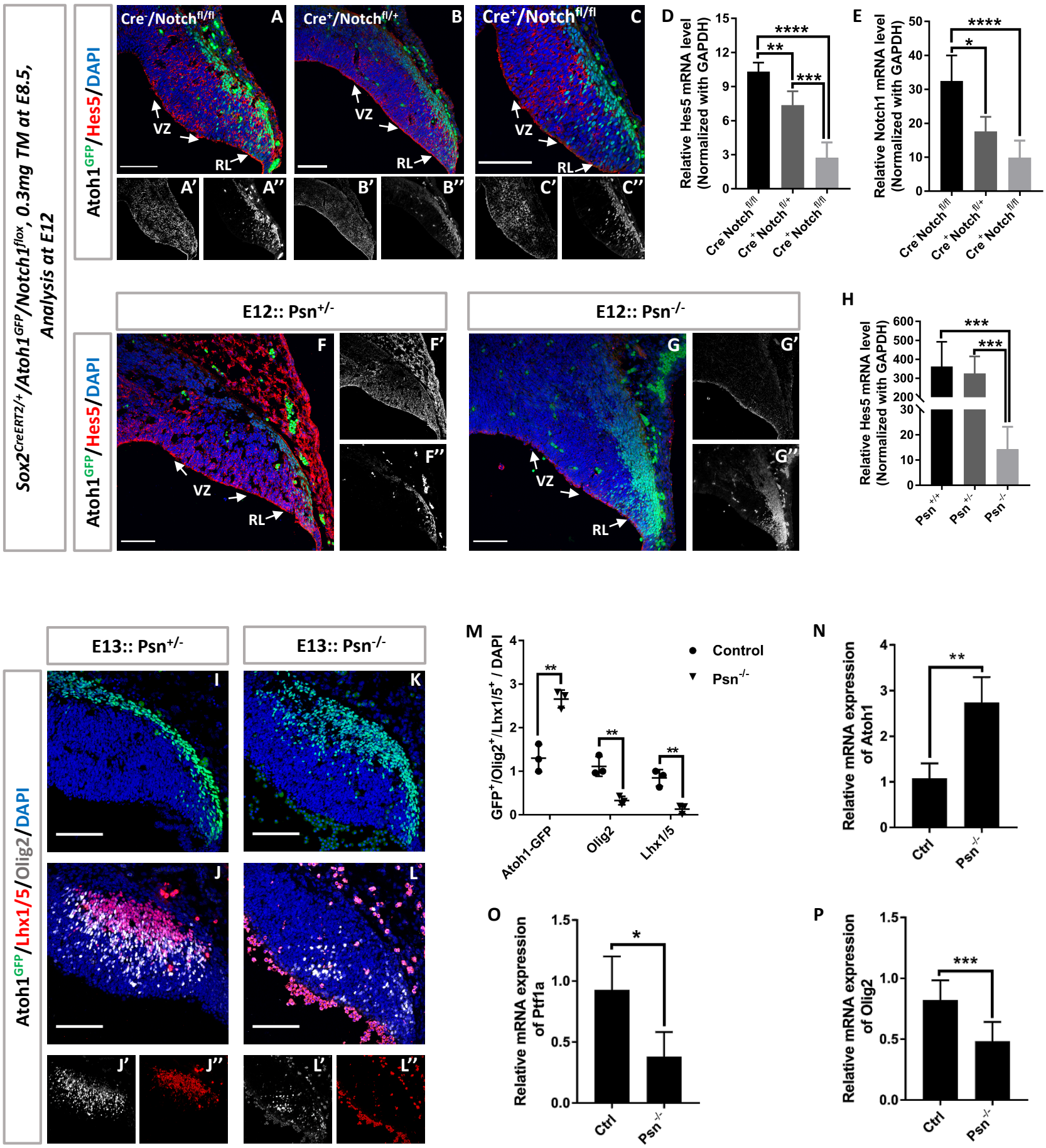

Figure S5: Notch loss of function does not affect cell proliferation and cell death in the cerebellar primordium

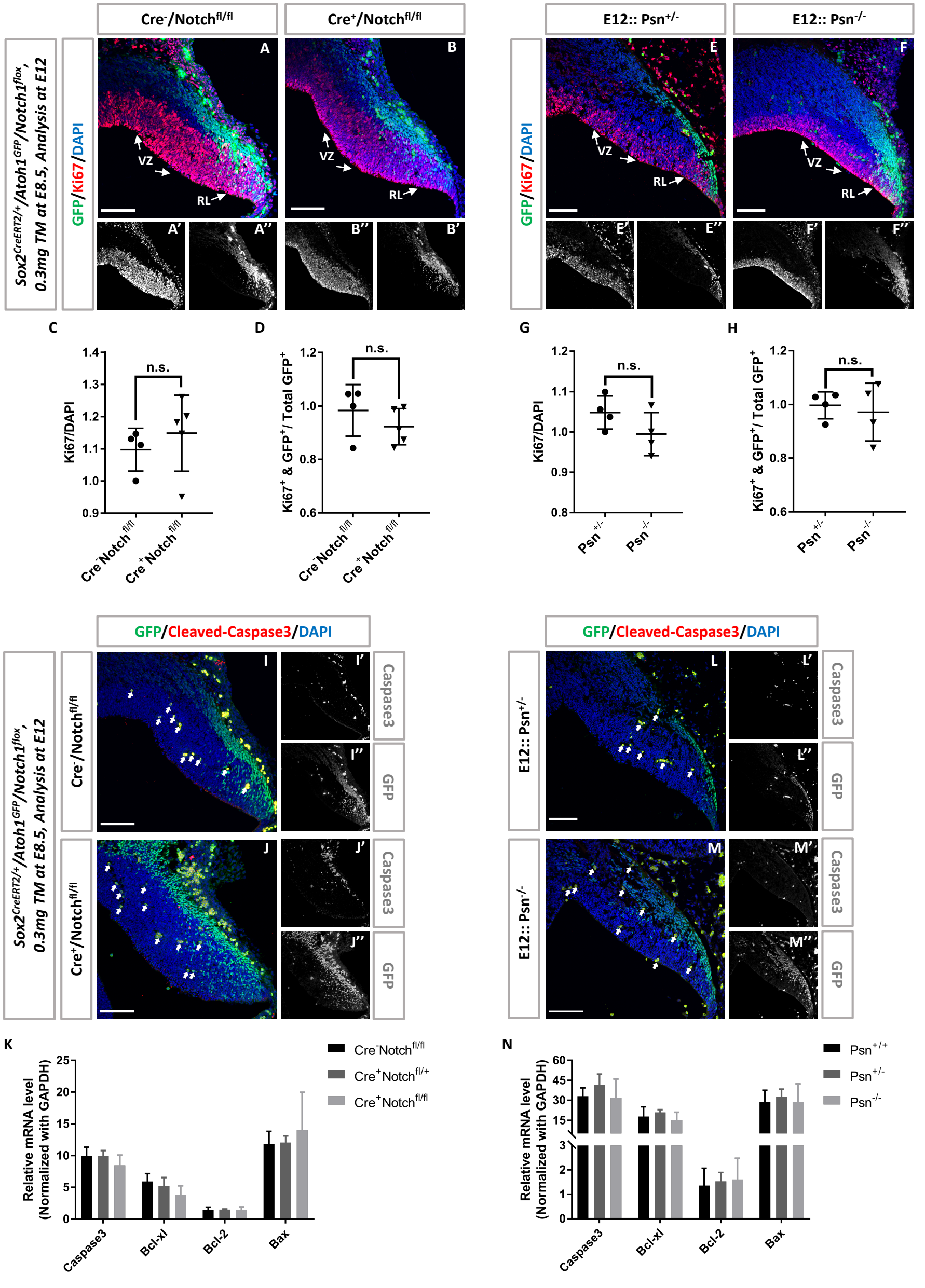

Figure S6: Notch inhibition in human cerebellar organoids and Notch GOF in ECPs in the mouse cerebellum

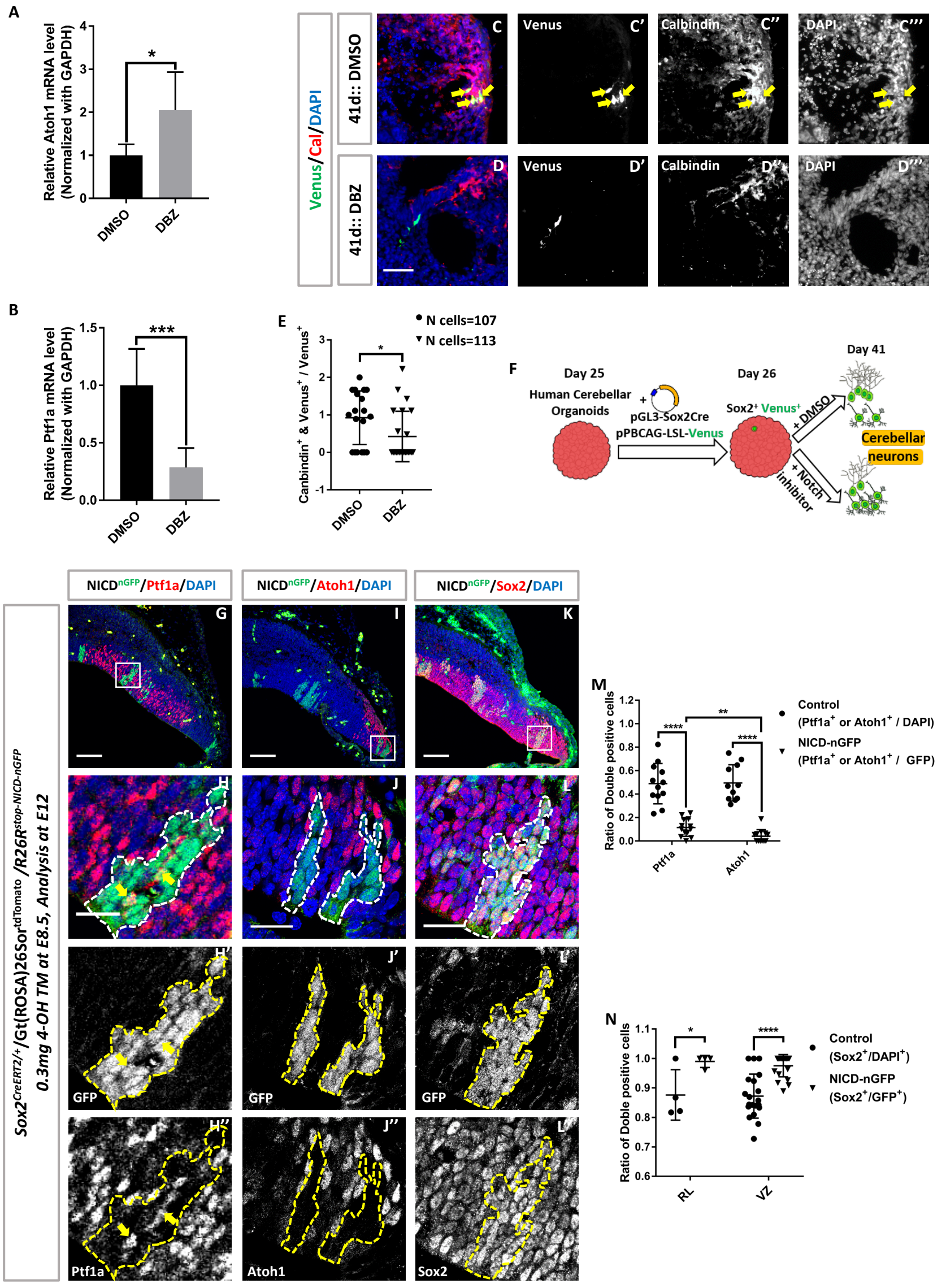

Figure S7: Notch GOF in ECPs shows lasting inhibition of their differentiation

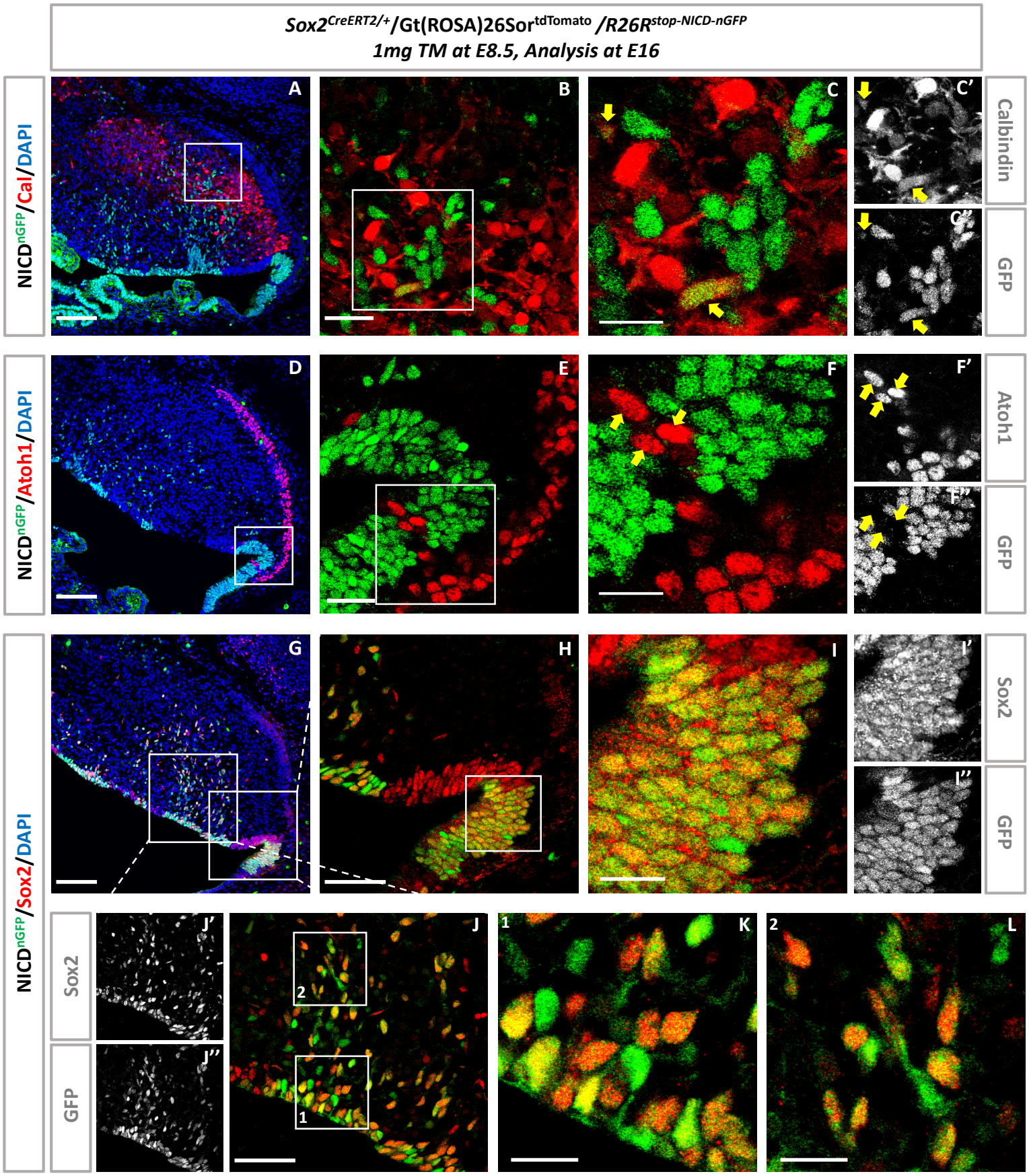

Table S1. MADM positive clones in mouse cerebellar hemisphere. Related to Figure 2.

E10-P21	Number				Ratio
Total hemisphere	76				
Total Clones	32				42.10%
Clones contain PC and GC	6	Yellow	Green and Red	Green or Red	18.75%
		3	2	1	
Clones contain PC only	24	Yellow	Green and Red	Green or Red	75.00%
		8	6	10	
Clones contain GC only	2	Yellow	Green and Red	Green or Red	6.25%
		2	0	0	
E11-P21	**Number**				**Ratio**
Total hemisphere	86				
Total Clones	23				26.74%
Clones contain PC and GC	3	Yellow	Green and Red	Green or Red	13.04%
		0	3	0	
Clones contain PC only	11	Yellow	Green and Red	Green or Red	47.83%
		3	4	4	
Clones contain GC only	9	Yellow	Green and Red	Green or Red	39.13%
		6	0	3	

Table S2. scRNAseq analysis of the mean level of Notch signaling related genes at E12 and E13. Related to Figure 4.

	Ptf1a only		Sox2 only		Atoh1 only	
	E12	E13	E12	E13	E12	E13
Number of cells	479	370	898	975	1375	665
Mean (Hes5)	2.0106	1.72	1.9952	2.1	1.1337	0.5
Mean (Hes1)	0.4288	0.6121	0.6756	1.1664	0.3307	0.2595
Mean (Notch1)	0.3358	0.3026	0.3659	0.3639	0.2625	0.0847
Mean (Dll1)	0.6101	0.8748	0.3115	0.2302	0.5419	0.3557
Mean (Dll3)	0.211	0.1502	0.1325	0.1115	0.8623	0.771
Mean (Dll4)	0.0012	0.0049	0.0022	0.005	0.0042	0.0172
Mean (Jag1)	0.0218	0.0241	0.0264	0.039	0.0328	0.0336
Mean (Jag2)	0	0	0.0007	0	0.0011	0

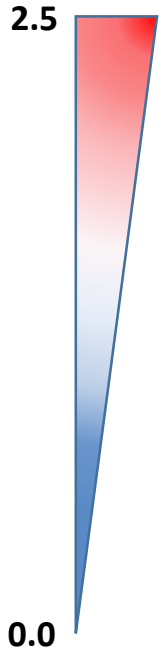

Table S3. Primers for mouse genotyping and RT-PCR. Related to STAR Methods.

Primers for genotyping		
Gene Name	Forward	Reverse
Cre	5’-CCAATTTACTGACCGTACACCAA-3’	5’-CTGATCCTGGCAATTTCGGCTA-3’
tdTom	WT-5’-AAGGGAGCTGCAGTGGAGTA-3’ Mut-5’-CTGTTCCTGTACGGCATGG-3’	WT-5’-CCGAAAATCTGTGGGAAGTC-3’ Mut-5’-GGCATTAAAGCAGCGTATCC-3’
Atoh1^{GFP}	WT-5’-GCGATGATGGCACAGAAGG-3’	WT-5’-GAAGGGCATTTGGTTGTCTCAG-3’ Mut-5’-AGGGTCAGCTTGCCGTAGGT-3’
Psn1	WT-5’-GTAGGGGATATGATTTTCTTTTTG-3’ Mut-5’-CATATACTGAAATCACAGCCAAG-3’	WT-5’-CCATTCGGGGAGGTACTTGATAA-3’ Mut-5’-CGGATCAAGCGTATGCAGCCG-3’
Notch^{flox}	5’-TGCCCTTTCCTTAAAAGTGG-3’	5’-GCCTACTCCGACACCCAATA-3’
NICD-nGFP	WT-5’-AAGGGAGCTGCAGTGGAGTA-3’ Mut-5’-TGGTATGCCTGACACTCACC-3’	WT-5’-CAGGACAACGCCCACACA-3’ Mut-5’-ACACCGGCCTTATTCCAA-3’
Primers for RT-PCR		
Gene Name	Forward	Reverse
Atoh1	5'- AGATCTACATCAACGCTCTGTC -3'	5'- ACTGGCCTCATCAGAGTCACTG -3'
Ptf1a	5'- GACGAGCAAGCAGAAGTAGAGT -3'	5'- GCAAGAGGAGGGAGACCATA -3'
hAtoh1	5'- GTAGACGGGATGCTCTCTCG -3'	5'- GCTGAAGTGAAGGAGTTGGG -3'
hPtf1a	5'- CCCCAGAAAACTCAACAGCA -3'	5'- AATCAGATCTTCAGCCGAGTC -3'
Olig2	5'- CGCAAGCTCTCCAAGATCG -3'	5'- CTCACCAGTCGCTTCATCTC -3'
Hes5	5'- AAGTACCGTGGCGGTGGAGATGC -3'	5'- CGCTGGAAGTGGTAAAGCAGCTT -3'
Notch1	5'- TGCCTGTGCACACCATTCTGC -3'	5'- CAATCAGAGATGTTGGAATGC -3'
Caspase3	5'- TGTCATCTCGCTCTGGTACG -3'	5'- AAATGACCCCTTCATCACCA -3'
Bcl-xl	5'- TTCGGGATGGAGTAAACTGG -3'	5'- AAGGCTCTAGGTGGTCATTCAG -3'
Bcl-2	5'- GATGACTTCTCTCGTCGCTAC -3'	5'- ACGCTCTCCACACACATGAC -3'
Bax	5'- TGGAGATGAACTGGACAGCA -3'	5'- CAAAGTAGAAGAGGGCAACCAC -3'
GAPDH	5'- GCTGCCAAGGCTGTGGGCAAG -3'	5'- GCCTGCTTCACCACCTTG -3'
hGAPDH	5'- TCCAGGAGCGAGATCCC -3'	5'- TTCTCCATGGTGGTGAAGACG -3'

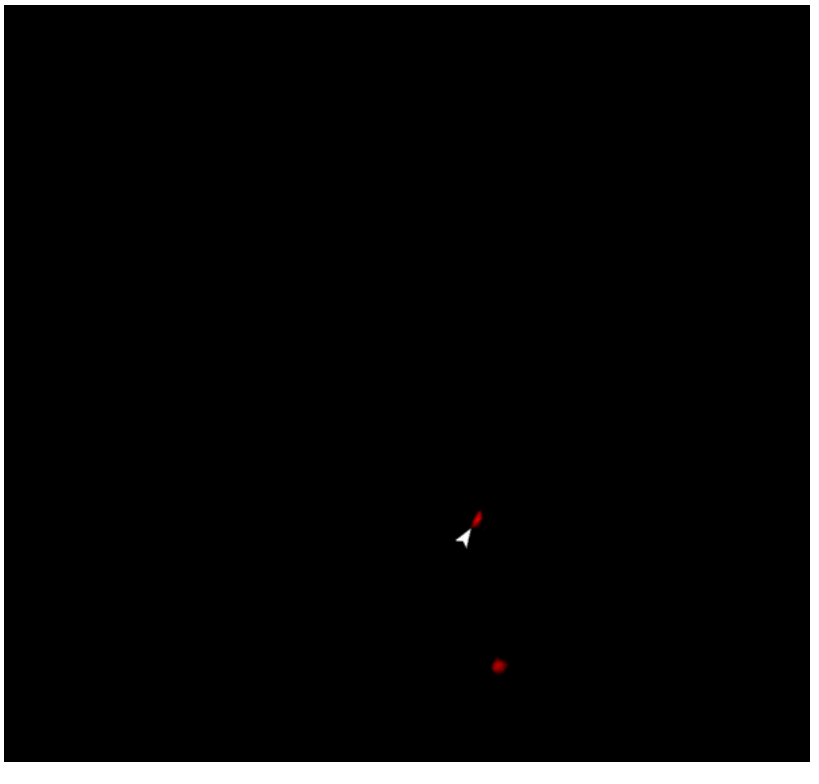

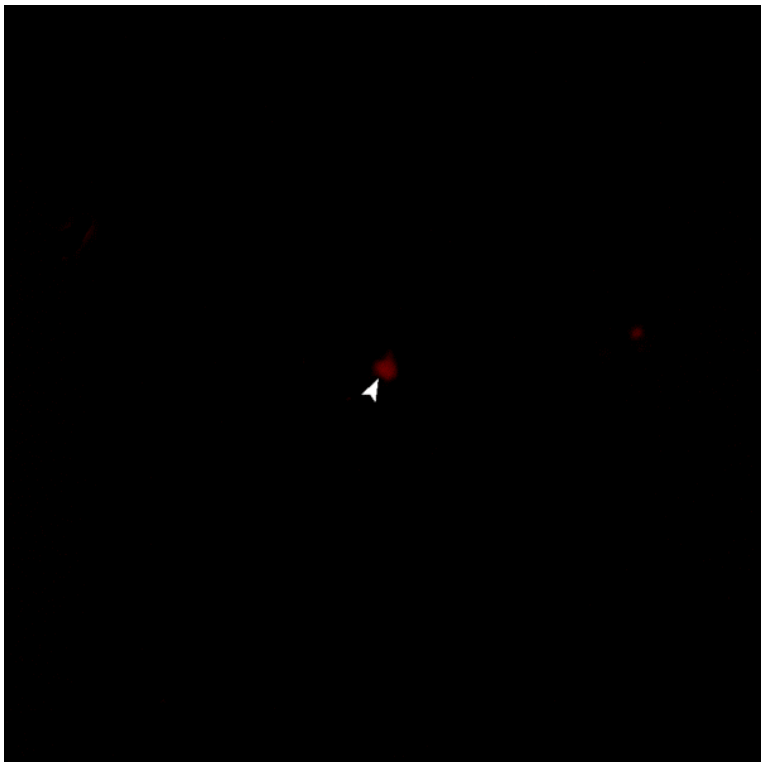

Movie S1-S2. A 12 days time-lapse sequence of live imaging for Sox2^{+} progenitors (Tomato^{+}, red) proliferation.